Peptide Conformations. 46.[1] Conformational Analysis of a Superpotent Cytoprotective Cyclic Somatostatin Analogue

Horst Kessler,* Jan Willem Bats, Christian Griesinger,† Sylvie Koll, Martin Will, and Klaus Wagner

Contribution from the Institut für Organische Chemie, Johann Wolfgang Goethe-Universität, D-6000 Frankfurt 50, West Germany. *Received March 27, 1987*

Abstract: Homo- and heteronuclear 1D- and 2D-NMR techniques have been used to assign proton and carbon resonances of *cyclo*(-D-Pro-Phe-Thr-Lys(Z)-Trp-Phe-) (**1**), a potent inhibitor of a transport system in hepatocytes. Independent confirmation of the NMR spectroscopic results was obtained from the analysis of three stereospecifically deuterated isotopomers of **1**. The conformational analysis of the backbone is based on evaluation of NOE effects in the rotating frame, chemical shift values, and their temperature dependence, and evaluation of coupling constants. The side-chain conformations are determined from homo- and heteronuclear coupling constants (via DISCO, E.COSY, and COLOC). A βI,βII′ structure is deduced for the hydrogen bridges Thr^3-CO-HN-Phe^6 and Phe^6-CO-HN-Thr^3. The derived conformation is refined by two molecular dynamics calculations using the GROMOS program in which the experimental distances obtained from ROE data are included as restraints. Whereas the first calculation (i) uses the conventional force field, the influence of the solvent environment is taken into account in the second calculation (ii) by reducing the charge at the NH protons, which are solvent exposed. The thus calculated conformation (ii) shows minor differences to the original βI,βII′ structure. In the conventional MD calculation bifurcated hydrogen bridges with additional γ^i turns are found. In the βI region the Thr hydroxyl group is found to be responsible for the compact packing of **1** because two acceptor hydrogen bonds from the NH protons of Trp^5 and Phe^6 and a donor bridge to the carbonyl oxygen of Phe^6 are formed. The solution structure of **1** was compared with the crystal structure of an analogue of **1** in which Lys(Z) was substituted by a Phe residue. A close similarity of both structures including the orientation of the side chains of the aromatic amino acids was found. However, a distinct difference between the structure in the crystal and in solution is expressed in the side-chain orientation of the Thr residue. The conformation of *cyclo*(-D-Pro-Phe-Thr-Phe-Trp-Phe-) (**7**) in Me_2SO solution is also very similar to the conformation of **1**.

In this paper we describe the conformation of the highly potent cytoprotective cyclic hexapeptide *cyclo*(-D-Pro^1-Phe^2-Thr^3-Lys^4-(Z)-Trp^5-Phe^6-) (**1**)[2] derived from NMR spectroscopy and refined by molecular dynamics calculation. **1** contains the slightly modified retrosequence 11-7 of somatostatin[3] (**2**), bridged by a D-proline. **1** is thus an analogue of one of the most thoroughly investigated peptide hormones with respect to biological activity.[4,5] Since **1** is a retroanalogue of somatostatin, it was not surprising that strong differences in biological activity of **1** and **2** were found. **1** has completely lost the hormonal effect of somatostatin (established by the suppression of the release of growth hormone, insulin, glucagon, gastrin, and others[6,7]). However, **1** turned out to be much more potent in cytoprotection than somatostatin. Cytoprotection means protection of organs and cells against various lesions;[8,9] in this case it is monitored in vitro by the inhibition of phalloidin or cholic acid uptake by isolated liver cells[2,10] (Table I).

It is of interest in this context that antamanide,[11,12] the cyclic decapeptide *cyclo*(-Val^1-Pro^2-Pro^3-Ala^4-Phe^5-Phe^6-Pro^7-Pro^8-Phe^9-Phe^{10}-) (**3**) isolated from the mushroom *Amanita phalloides*,[12] shows a cytoprotective activity similar to that of **1**, although the constitution of the two peptides have no apparent similarity. Since molecular shape correlates with biological activity (rather than constitution), it is necessary to determine the conformation of these two different peptides and to compare them to reveal common structural features which may account for the similar pharmacological activity. The conformation of antamanide will be published elsewhere.[13,14] We present here the conformation of **1** in Me_2SO solution. **1** has not yet been crystallized; NMR spectroscopy is therefore the only way to determine its structure. This was done using the most recent one- and two-dimensional NMR techniques.[14-16]

Different techniques which provide sometimes similar information are compared and evaluated with respect to reliability, applicability, and relevance for structure determination. An additional check of the NMR results was possible by the parallel investigation of three isotopomers of **1**: *cyclo*(-D-Pro^1-Phe^2-Thr^3-Lys^4(Z)-Trp^5-(*S*,*S*)-(α,β-^{2}H)-Phe^6-) (**4**), *cyclo*(-D-Pro^1-Phe^2-Thr^3-Lys^4(Z)-(*S*,*S*)-(α,β-^{2}H)-Trp^5-Phe^6-) (**5**), and *cyclo*(-D-Pro^1-(*S*,*S*)-(α,β-^{2}H)-Phe^2-Thr^3-Lys^4(Z)-Trp^5-Phe^6-) (**6**). This

Table I. 50% Inhibition of Radioactive Cholate Uptake in Isolated Liver Cells[a]

Compound		(μmol)
Title compound 1	D-Pro-Phe-Thr | | Phe-Trp-Lys(Z)	1.5
Somatostatin 2	H-Ala-Gly-Cys-Lys-Asn-Phe-Phe-Trp | HO-Cys-Ser-Thr-Phe-Thr-Lys	220.0
Antamanide 3	Val-Pro-Pro-Ala-Phe | | Phe-Phe-Pro-Pro-Phe	8.0
(Phe^4)-derivative of 1	D-Pro-Phe-Thr | Phe-Trp-Phe	2.0
8	D-Pro-Phe-Phe | | Phe-Phe-Pro	2.5
9	Pro-Pro-Phe \ / Gly-Phe	b)

[a] This test is described in ref 2. [b] No observable effect.

† Present address: Laboratorium für Physikalische Chemie, Eidgenössische Technische Hochschule, CH-8092 Zürich, Switzerland.

(1) Lautz, J.; Kessler, H.; Boelens, R.; Kaptein, R.; van Gunsteren, W. F. *Int. J. Peptide Protein Res.* **1987**, *30*, 404-414.
(2) Ziegler, K.; Frimmer, M.; Kessler, H.; Damm, I.; Eiermann, V.; Koll, S.; Zarbock, J. *Biochim. Biophys. Acta* **1985**, *845*, 86-93.
(3) Brazeau, P.; Vale, W.; Burgus, R.; Ling, N.; Butcher, M.; Rivier, J.; Guillemin, R. *Science* **1973**, *179*, 77-79.
(4) (a) Reichlin, S.; *New Engl. J. Med.* **1983**, *309*, 1495-1501. (b) Reichlin, S. *Ibid.* **1983**, *309*, 1556-1563.
(5) Proceedings of the 2nd International Symposium on Somatostatin held June 1-3, 1981, Athens (Greece); Raptis, S., Rosenthal, J., Gerich, J., Eds.; Attempto Verlag: Tübingen, Germany, 1984.
(6) Koerker, D. J.; Ruch, W.; Chideckel, E.; Palmer, J.; Goodner, C. J.; Ensick, J.; Gale, C. C. *Science* **1974**, *184*, 482-484.
(7) Unger, R. H. *Diabetes* **1976**, *25*, 36.
(8) Szabo, S.; Usadel, K. H. *Experientia* **1982**, *38*, 254-255.
(9) Usadel, K. H.; Kessler, H.; Rohr, G.; Kusterer, K.; Palitsch, K. D.; Schwedes, U. *Klin. Wochenschr.* **1986**, *64*, 59-63.
(10) Kessler, H.; Klein, M.; Müller, A.; Wagner, K.; Bats, J. W.; Ziegler, K.; Frimmer, M. *Angew. Chem., Int. Ed. Engl.* **1986**, *25*, 997-999.
(11) Wieland, T.; Lüben, G.; Ottenheym, H.; Faesel, J.; de Vries, J. X.; Konz, W.; Prox, A.; Schmid, A. *Angew. Chem., Int. Ed. Engl.* **1968**, *7*, 204-208.

0002-7863/88/1510-1033$01.50/0

Table II. Methodology for the Solid-Phase Synthesis of **1**

step	reagent	no. of cycles	time (min)
1	CH_2Cl_2	3	3
2	10% trifluoroacetic acid, 0.5% methanesulfonic acid, CH_2Cl_2	1	30
3	CH_2Cl_2/dioxane, 1:1	3	3
4	CH_2Cl_2/methanol, 1:1	3	3
5	CH_2Cl_2	3	3
6	10% diisopropylethylamine, CH_2Cl_2	3	5
7	CH_2Cl_2	2	3
8	CH_2Cl_2/dimethylformamide, 4:1	2	3
9	1 equiv Boc-amino acid, 1 equiv DCC, 1 equiv HOBt, CH_2Cl_2/dimethylformamide, 4:1	1	180
10	CH_2Cl_2/methanol/dimethylformamide, 3:1:1	6	3

extra synthetic effort was made to obtain the conformationally relevant NMR parameters as completely as possible. This is not only required in order to determine a reliable 3D structure, but also to prove conformational homogeneity.[14,17,18] The assignment of the NMR active nuclei to the molecular constitution can be done exclusively on the basis of connectivity information via scalar coupling. Rotating frame NOE effects (ROE) obtained from ROESY spectra then are used for the determination of proton distances. Those distances enter molecular dynamics (MD) calculations as restraints. Two different calculations were performed: besides the conventional restraint MD, a second calculation was done in which the charge was released at the solvent-exposed NH protons monitored experimentally from their temperature dependencies. The resulting backbone conformation is checked by further NMR parameters. Homo- and heteronuclear scalar couplings serve to determine torsional angles of the side chains. The thus obtained refined conformation is compared with the solid-state structure of an analogue of **1**, in which the Lys^4(Z) is substituted by a Phe residue. This compound (**7**) exhibits extremely similar NMR spectra to **1**, which indicate similar conformations of both cyclopeptides in solution. Molecular flexibility of the title compound is probed with T_1 relaxation times of the carbon nuclei.

Synthesis

The synthesis of the cyclic hexapeptides **1** and **7** was carried out by the solid-phase method introduced by Merrifield[19] (Table II). The synthesis of the deuterated isomers **4** – **6** followed the same procedure. Boc-Lys(Z)-OH (**7**: Boc-Phe-OH) was esterified to hydroxymethylated resin as described previously;[20,21] the chain was extended by successive coupling using Boc-Thr-OH, Boc-Phe-OH, Boc-D-Pro-OH, Boc-Phe-OH and Boc-Trp-OH. The peptide was cleaved from the resin via hydrazinolysis. After removing the N-terminal Boc group by treatment with trifluoroacetic acid, the peptide was cyclized using the azide method according to Medzihradszky.[22]

Boc-(*S*,*S*)-(α-^{2}H,β-^{2}H)-Phe-OH was prepared by deuteration of *N*-acetyl-Z-dehydrophenylalanine[23] and cleavage of the α-*S* enantiomer by porcine kidney acylase.[24] *N*-Acetyl-Z-dehydrophenylalanine was easily available by the reaction of Ac-Gly-OH and benzaldehyde, and hydrolysis of the corresponding azlactone.[25]

The synthesis of peptide **5** was carried out using a racemic mixture of (*R*,*R*)- and (*S*,*S*)-Boc-(α-^{2}H,β-^{2}H)-Trp-OH, which was prepared by deuteration of *N*-acetyl-Z-dehydrotryptophan[26] and exchange of the N-terminal protecting group. The final product, isomer **5**, was separated by Sephadex LH 20 gel chromatography. Both epimeric peptides, **5** and *cyclo*(-D-Pro^1-Phe^2-Thr^3-Lys^4(Z)-D-(*R*,*R*)-(α,β-^{2}H)-Trp^5-Phe^6-), were obtained in comparable yields.

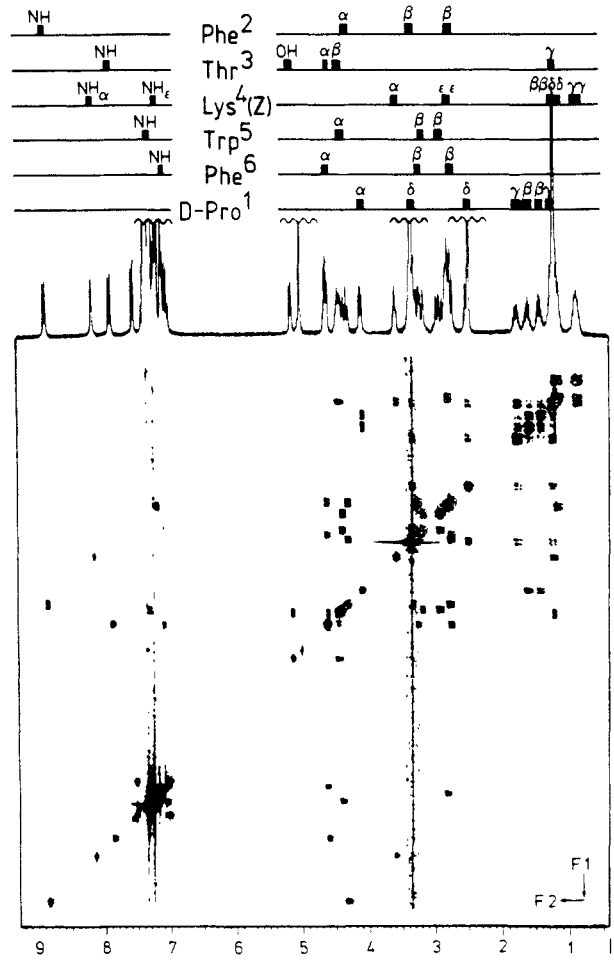

Figure 1. 300-MHz DQF-H,H-COSY spectrum of *cyclo*(-D-Pro-Phe-Thr-Lys(Z)-Trp-Phe-) (**1**) in Me_2SO solution at 300 K. Assignments and the 1D spectrum are given above.

Assignments

The assignment of almost all NMR active nuclei is described in this section. It is mainly based on connectivity information transmitted via homo- and heteronuclear scalar couplings. The proton signals are assigned in a conventional double quantum filtered (DQF) H,H-COSY spectrum[27,28] (Figure 1).

The residues of D-Pro^1, Thr^3, Lys^4(Z), and Trp^5 can be identified directly from their coupling patterns. The digitization in the phase-sensitive DQF-COSY spectrum is sufficiently high to resolve the cross peak from the small ^4J coupling between H$^\beta$ and H$'_2$

(12) Wieland, T. *Peptides of Poisonous Amanita Mushrooms*; Rich, A., Ed.; Springer Verlag: New York, 1986.
(13) Kessler, H.; Müller, A. *J. Org. Chem.*, submitted for publication.
(14) Kessler, H.; Bermel, W.; Müller, A.; Pook, K. H. *The Peptides: Analysis, Synthesis, Biology*; Udenfriend, S., Meienhofer, J., Hruby, V., Eds.; Verlag Chemie: Weinheim, 1986; Vol. 7, pp 437–472.
(15) Kessler, H.; Bermel, W. *Methods in Stereochemical Analysis*; Takeuchi, A., Marchand, P., Eds.; Verlag Chemie: Weinheim, 1986; pp 179–205.
(16) Kessler, H.; Oschkinat, H.; Loosli, H. R. *Methods in Stereochemical Analysis*; Croasmun, W. R., Carlson, R. M., Eds.; VCH: Deerfield Beach, FL, 1987; Vol. 9, pp 259–299.
(17) Kessler, H. *Angew Chem., Int. Ed. Engl.* **1982**, *21*, 512–523.
(18) Kessler, H.; Wagner, K.; Will, M. *Trends in Medicinal Chemistry*; Mutschler, E., Winterfeld, E., Eds., VCH: Weinheim, 1987; pp 143–157.
(19) Merrifield, R. B. *J. Am. Chem. Soc.* **1963**, *85*, 2149–2154.
(20) Kessler, H.; Bernd, M.; Damm, I. *Tetrahedron Lett.* **1982**, *23*, 4685–4688.
(21) Kessler, H.; Eiermann, V. *Tetrahedron Lett.* **1982**, *23*, 4689–4692.
(22) Klausner, Y. S.; Bodanszky, M. *Synthesis* **1974**, 549–559.
(23) Kirby, G. W.; Michael, J. *J. Chem. Soc., Perkin Trans.* **1973**, *1*, 115–120.
(24) Birnbaum, M.; Levintow, L.; Kingsley, R. B.; Greenstein, J. P. *J. Biol. Chem.* **1952**, *194*, 455–470.
(25) Herbst, R. M.; Shemin, D. *Organic Syntheses*, Collect Vol. 2; Wiley: New York, 1943; pp 1–3.
(26) Hengartner, U.; Valentine, D.; Johnson, K. K.; Larscheid, M. E.; Pigott, F.; Scheidl, F.; Scott, J. W.; Sun, R. C.; Townsend, J. M.; Williams, T. H. *J. Org. Chem.* **1979**, *44*, 3741–3747.
(27) Piantini, U.; Sørensen, O. W.; Ernst, R. R. *J. Am. Chem. Soc.* **1982**, *104*, 6800–6801.
(28) Rance, M.; Sørensen, O. W.; Bodenhausen, G.; Wagner, G.; Ernst, R. R.; Wüthrich, K. *Biochem. Biophys. Res. Commun.* **1983**, *117*, 479–485.

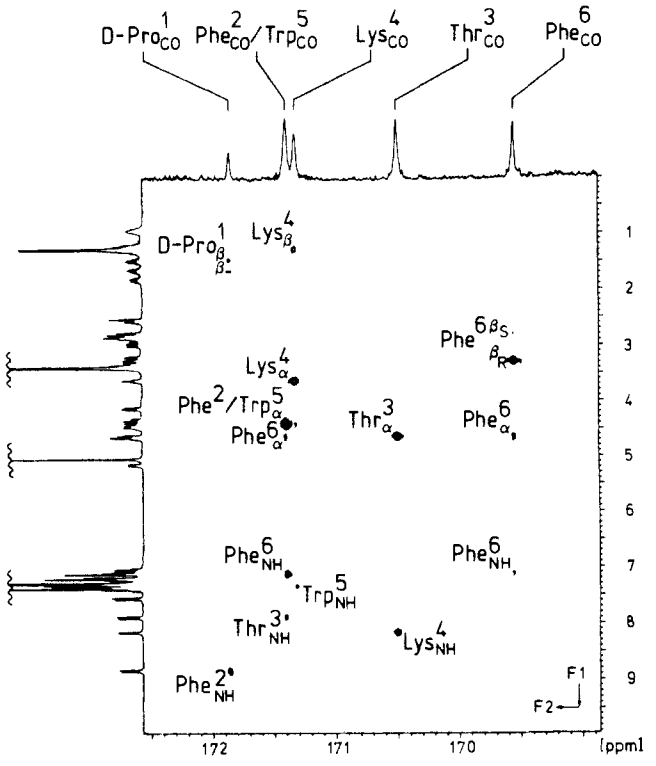

Figure 2. 300-MHz H,C-COLOC spectrum of the carbonyl carbons of *cyclo*(-D-Pro-Phe-Thr-Lys(Z)-Trp-Phe-) (**1**) in Me_2SO solution at 300 K with assignments of the cross peaks and carbonyl carbon resonances in the 1D spectrum above.

of Trp[5] and thus identify this residue. Therefore, it is not necessary to perform a delayed COSY[29] to detect the small couplings between aromatic protons and β protons.[30] The characteristic high-field shift of the Trp[5]-C$^{\beta}$ resonance[31] is another feature to distinguish Phe and Trp resonances in an H,C-COSY spectrum[32] (see supplementary material). The proton chemical shifts of the indole resonances were obtained from the DQF-COSY spectrum, whereas the resonances of the ortho (o), meta (m), and para (p) protons in the phenyl rings were assigned via an H,C-COSY spectrum (see supplementary material). The two Phe residues remain indistinguishable at this stage. The distinction between the aromatic amino acid resonances results from the sequence analysis of the peptide. For this purpose proton–carbon long-range couplings (observed in the H,C-COLOC spectrum,[33-35] Figure 2) as well as ROE (rotating frame NOE) effects (observed in the ROESY spectrum,[36-40] Figure 3) are exploited. The assignment of some of the carbonyl carbons in the H,C-COLOC spectrum follows directly from their cross peaks to the protons whose chemical shifts are already known from the DQF-COSY spectrum. The coupling to β protons unequivocally assigns the carbonyls of D-Pro,[1] Lys[4](Z), and one of the Phe residues (Phe[6], although this

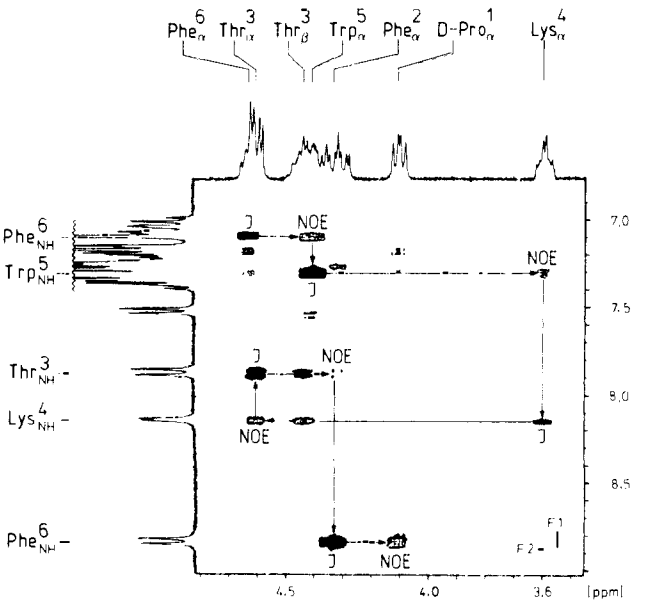

Figure 3. Part of the 300-MHz ROESY spectrum of *cyclo*(-D-Pro-Phe-Thr-Lys(Z)-Trp-Phe-) **1** in Me_2SO solution at 300 K. This spectrum shows NH,H$^{\alpha}$ correlations via *J* transfer (positive) and NOE transfer (negative). Positive cross peaks are indicated as filled contours. Sequence analysis is possible following the arrows.

Table III. ^{1}H NMR Chemical Shifts (δ) of **1** in Me_2SO Solution at 300 K

	D-Pro[1]	Phe[2]	Thr[3]	Lys[4](Z)	Trp[5]	Phe[6]
NH		8.81	7.86	8.12	7.32	7.08
H$^{\alpha}$	4.11	4.32	4.61	3.60	4.40	4.62
H$^{\beta pro\text{-}S}$	1.44	3.33		1.22[a]	3.20	2.76
H$^{\beta pro\text{-}R}$	1.62	2.77	4.45		2.93	3.26
H$^{\gamma pro\text{-}S}$	1.78		1.24	0.89[a]		
H$^{\gamma pro\text{-}R}$	1.26					
H$^{\delta pro\text{-}S}$	2.52			1.23[a]		
H$^{\delta pro\text{-}R}$	3.36					
H$^{\epsilon}$, OH			5.12	2.80[a]		
Z_{Bzl}				5.01		
NH$^{\epsilon}$,NH$_{indole}$				7.19	10.82	
H^{o},H$'_2$		7.25		7.34	7.10	7.17
H^{m},H$'_4$		7.26		7.36	7.53	7.30
H^{p},H$'_5$		7.26		7.29	7.01	7.18
H$'_6$					7.07	
H$'_7$					7.34	

[a] Degenerated protons.

is not known at this stage) whose α-proton resonance overlaps with the Thr[3]-H$^{\alpha}$ resonance.

Therefore the Thr[3]-C$'$ can be assigned from the Thr[3]H$^{\alpha}$–C$'$ cross peak, even though the α protons of Thr[3] and Phe[6] overlap. Now all carbonyl carbons are assigned except those of the other Phe (Phe[2]) and of Trp[5]. The remaining ^{13}C signal at 171.4 ppm therefore contains these missing resonances. The two (NH-C$'$) cross peaks Thr[3]NH-Phe[2]C$'$ and Phe[6]NH-Trp[5]C$'$ immediately provide the distinction between Phe[2] and Phe[6] because such couplings can only occur between adjacent amino acids. The remaining sequence relations can be derived from the spectrum in a similar way.

Independent proof of these assignments was obtained by the rotating frame cross-relaxation experiment (ROESY). This experiment was applied instead of the NOESY experiment,[41-43] because **1** shows only a few small NOE effects at 300- or 500-MHz spectrometer frequency due to unfavorable correlation times

(29) Bax, A.; Freeman, R. *J. Magn. Reson.* **1981**, *44*, 542–561.
(30) Kessler, H.; Hölzemann, G.; Zechel, C. *Int. J. Peptide Protein Res.* **1985**, *25*, 267–279.
(31) Kessler, H.; Bernd, M.; Kogler, H.; Zarbock, J.; Sørensen, O. W.; Bodenhausen, G.; Ernst, R. R. *J. Am. Chem. Soc.* **1983**, *105*, 6944–6952.
(32) Freeman, R.; Morris, G. A. *J. Chem. Soc., Chem. Commun.* **1978**, 684–686.
(33) Kessler, H.; Griesinger, C.; Zarbock, J.; Loosli, H. R. *J. Magn. Reson.* **1984**, *57*, 331–336.
(34) Kessler, H.; Griesinger, C.; Lautz, J. *Angew. Chem., Int. Ed. Engl.* **1984**, *23*, 444–445.
(35) Kessler, H.; Bermel, W.; Griesinger, C.; Kolar, C. *Angew. Chem., Int. Ed. Engl.* **1986**, *25*, 342–344.
(36) Bothner-By, A. A.; Stephens, R. L.; Lee, J.; Warren, C. D.; Jeanloz, R. W. *J. Am. Chem. Soc.* **1984**, *106*, 811–813.
(37) Bax, A.; Davis, D. G. *J. Magn. Reson.* **1985**, *63*, 207–213; **1985**, *65*, 355–360.
(38) Neuhaus, D.; Keeler, J. *J. Magn. Reson.* **1986**, *68*, 568–574.
(39) Kessler, H.; Griesinger, C.; Kerssebaum, R.; Wagner, K.; Ernst, R. R. *J. Am. Chem. Soc.* **1987**, *109*, 607–609.
(40) Griesinger, C.; Ernst, R. R. *J. Magn. Reson.* **1987**, *75*, 261–271.
(41) Jeener, J.; Meier, B. H.; Bachmann, P.; Ernst, R. R. *J. Chem. Phys.* **1979**, *71*, 4546–4553.
(42) Kumar, A.; Wagner, G.; Ernst, R. R.; Wüthrich, K. *J. Am. Chem. Soc.* **1981**, *103*, 3654–3658.
(43) Macura, S.; Wüthrich, K.; Ernst, R. R. *J. Magn. Reson.* **1982**, *47*, 351–357.

Table IV. ^{13}C Chemical Shifts (δ) of **1** in Me_2SO Solution at 300 K

	D-Pro[1]	Phe[2]	Thr[3]	Lys[4](Z)	Trp[5]	Phe[6]
C^α	60.3	54.6	56.8	55.6	55.2	53.5
C^β	28.2	35.9	68.9	29.9	28.2	38.3
C^γ	24.8		19.6	22.4		
C^δ	47.1			29.4		
C^ϵ				40.1		
C′	171.9	171.4	170.5	171.3	171.4	169.5
C'^ϵ				156.3		
C^o		129.0		127.9		129.6
C^m		128.3		128.5		128.5
C^p		127.1		127.9		126.3
C^i		138.9		137.4		136.3
C'_2					123.4	
C'_3					110.3	
C'_{3a}					136.3	
C'_4					118.1	
C'_5					118.6	
C'_6					121.1	
C'_7					111.6	
C'_{7a}					127.4	

for peptides of this size. In the section of the ROESY spectrum showing (NH–H^α) connectivities (Figure 3), cross peaks due to a ROE (rotating frame Overhauser enhancement) effect are negative with respect to the diagonal (open contours), while J connectivity peaks (TOCSY peaks[44]) have positive intensity (filled contours). With these two types of cross peaks the whole sequence can be traced out (see Figure 3).

Starting at the Phe[6]NH-Phe[6]H^α J cross peak the horizontally connected ROE peak (Phe[6]NH-Trp[5]H^α) indicates the connectivity Phe[6]-Trp[5]. Following now a vertical line the Trp[5]NH-Trp[5]H^α J cross peak is found. Again following the horizontal line, the next ROE peak (Trp[5]NH-Lys[4]H^α) is obtained providing the Trp[5]-Lys[4] connectivity. Repetition of this procedure assigns the whole sequence up to the D-Pro[1] residue. The missing Phe[6]-D-Pro[1] connectivity is established by the cross peaks between Phe[6]H^α and both D-Pro[1]H^δ resonances (not seen in this section of the spectrum in Figure 3). We should mention that this ROESY spectrum was obtained from mixing with a train of 180° pulses which effectively enables transfer via J couplings.[39,40] This version of the ROESY experiment can, however, not be used for quantitative evaluation (see below).

Finally, a third independent proof of the sequential assignments is obtained by the ^1H NMR spectra of the stereoselectivity deuterated isomers **4–6** (Figure 4). The ^1H chemical shift data are collected in Table III. The assignment of the carbon signals was obtained from an H,C-COSY spectrum (see supplementary material) for the aliphatic carbon resonances and an H,C-COLOC spectrum for the carbonyl resonances (see above). The assignment of the aromatic carbons in a peptide is not often performed. However, T_1 relaxation times of those carbons provide information about the flexibility of the side chains and local correlation times which are of importance for the quantitative evaluation of NOE effects. The chemical shifts of the aromatic carbon signals were determined by an H,C-COSY spectrum (see supplementary material) and an H,C-COLOC spectrum.

The protonated carbons of the indole ring were identified in the H,C-COSY spectrum with the knowledge of the chemical shifts of the directly bound protons. The other carbon signals of the indole system were assigned with the help of characteristic long-range couplings (Trp[5]C'_3–H^β, Trp[5]C'_{3a}–H'_4) according to the rule $^2J(C,H) \approx 0$ and $^3J(C,H) > 4$ Hz for aromatic systems[45] in the H,C-COLOC spectrum. Especially useful are the long-range couplings of the $H^\beta C^i$ (i = ipso) and $H^\beta C^o$ cross peaks, because they provide the sequence assignment of the phenyl rings. In addition, the H^mC^i and H^pC^m cross peaks in a H,C-COLOC spectrum together with assignments via $^1J(C,H)$ couplings from the H,C-COSY spectrum yield the full assignment of all protons and carbons in the phenyl rings (Tables III and IV).

The assignment of the protonated nitrogen signals was obtained from an H,N-COSY spectrum[46] (see Experimental Section).

Table V. Vicinal Coupling Constants, Corresponding φ Angles and Theoretical Angles[a] of Four Different β-Turn Types and the Two Different γ-Turn Types

residue	$^3J(NH,H^\alpha)$ [Hz]	φ (deg)
Phe[2]	8.9[b]	−100, −140
Thr[3]	9.7[b]	−110, −130
Lys[4]	3.4[b]	11, 109, −63, −177
Trp[5]	8.9[c]	−100, −140
Phe[6]	5.8[c]	29, 91, −78, −162

turn	position	φ (deg)	turn	position	φ (deg)
βI	$i+1$	−60	βII′	$i+1$	60
	$i+2$	−90		$i+2$	−80
βI′	$i+1$	60	γ	$j+1$	85
	$i+2$	90	γ^i	$j+1$	−85
βII	$i+1$	−60			
	$i+2$	80			

[a] See ref 67. [b] Obtained from the 1D spectrum of **1**. [c] Obtained from DQF-COSY spectrum via the DISCO procedure.

Table VI. $J(H^\alpha,H^\beta)$ Coupling Constants Obtained from the E.COSY Spectrum of **1** and Rotamer Populations of Phe[2], Thr[3], Trp[5], and Phe[6] Residues

	Phe[2]	Thr[3]	Trp[5]	Phe[6]
$J(H^\alpha H^{\beta pro\text{-}S})$ (Hz)	3.1 (2.9)[a]		4.2 (4.0)	9.0 (9.1)
$J(H^\alpha H^{\beta pro\text{-}R})$ (Hz)	11.5 (11.8)	3.5	10.9 (11.1)	4.5 (4.2)
P_I	0.80 (0.84)	predominant	0.75 (0.78)	0.17 (0.14)
P_{II}	0.05 (0.02)	minor	0.15 (0.12)	0.58 (0.59)
P_{III}	0.15 (0.13)	minor	0.10 (0.10)	0.25 (0.27)

[a] The values given in parentheses are obtained via the DISCO technique.

Extraction of Conformationally Relevant NMR Parameters

The analysis of the backbone conformation is based on chemical shift values and their temperature dependence, NOE effects, and a quantitative evaluation of coupling constants. The conformations of the side chains are derived from homo- and heteronuclear coupling constants as well as from ROE effects. T_1 relaxation times of ^{13}C resonances serve as a probe of molecular flexibility.

The NH,H^α coupling constants of Phe[2], Thr[3], and Lys[4] are directly determined from the one-dimensional spectrum of **1**. Those of Trp[5] and Phe[6] and the H^α,H^β couplings of the three aromatic amino acid residues are obtained from the DQF-COSY spectrum using the DISCO technique (*di*fferences and *s*ums in *COS*Y spectra)[47–49] and are collected in Tables V and VI (see also Figure 5).

We also applied the E.COSY[50–52] technique for the extraction of coupling constants. A section of the E.COSY spectrum featuring the characteristic cross-peak patterns in comparison to DQF-COSY is given in Figure 6. The coupling constants can be extracted from this spectrum with high accuracy (Table VI). The coupling constants extracted from DISCO and E.COSY agree to a large extent. For practical application we found the following: the DISCO procedure is applied on conventional double-quantum-filtered phase-sensitive COSY spectra. It involves coaddition over the whole cross peak and thus achieves a good signal-to-noise ratio for the pseudo-1D spectrum (Figure 5). DISCO can be successfully applied when at least three protons couple to one proton or when at least three protons are mutually coupled. This

(44) Braunschweiler, L.; Ernst, R. R. *J. Magn. Reson.* **1983**, *53*, 521–528.
(45) Kalinowski, H. O.; Berger, S.; Braun, S. *13C-NMR-Spektroskopie*; Georg Thieme Verlag: Stuttgart, New York, 1984.
(46) Kessler, H.; Hehlein, W.; Schuck, R. *J. Am. Chem. Soc.* **1982**, *104*, 4534–4540.
(47) Oschkinat, H.; Freeman, R. *J. Magn. Reson.* **1984**, *60*, 160–169.
(48) Kessler, H.; Oschkinat, H. *Angew. Chem., Int. Ed. Engl.* **1985**, *24*, 690–692.
(49) Kessler, H.; Müller, A.; Oschkinat, H. *Magn. Reson. Chem.* **1985**, *23*, 844–852.
(50) Griesinger, C.; Sørensen, O. W.; Ernst, R. R. *J. Am. Chem. Soc.* **1985**, *107*, 6394–6396.
(51) Griesinger, C.; Sørensen, O. W.; Ernst, R. R. *J. Chem. Phys.* **1986**, *85*, 6837.
(52) Griesinger, C.; Sørensen, O. W.; Ernst, R. R. *J. Magn. Reson.*, in press.

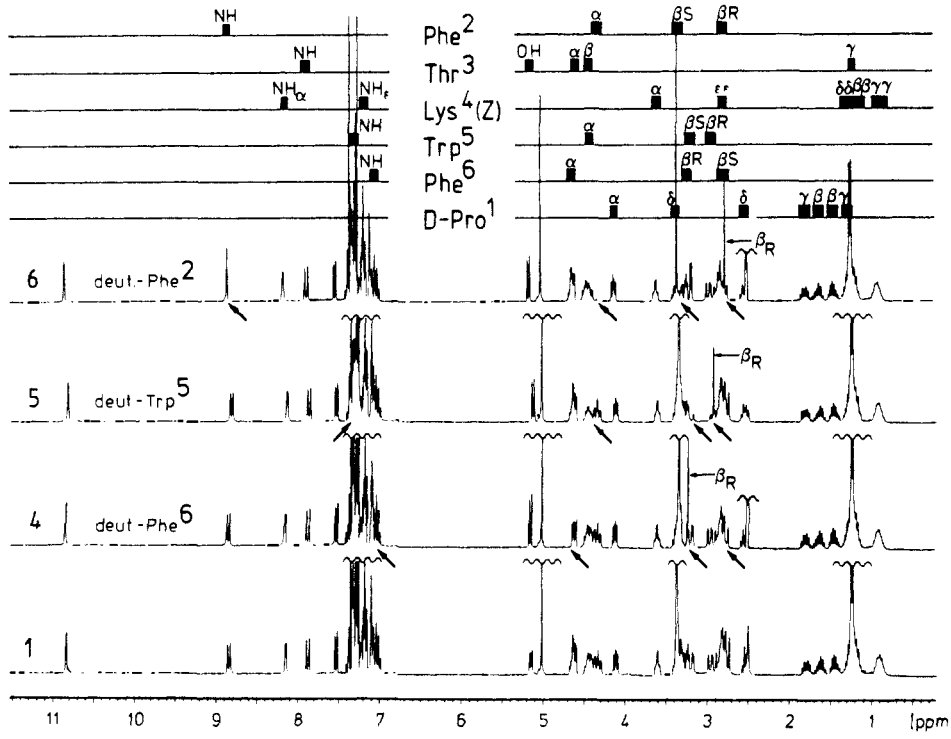

Figure 4. 270-MHz ^{1}H spectra of **1** and the stereoselectively deuterated isotopomers **4** – **6**. Deuteration was always done in α and β pro-S positions of the aromatic amino acids. Arrows point at the NH (singlet), the missing H^{α} resonances, the missing $H^{\beta pro\text{-}S}$ resonance, and the $H^{\beta pro\text{-}R}$ resonance (singlet).

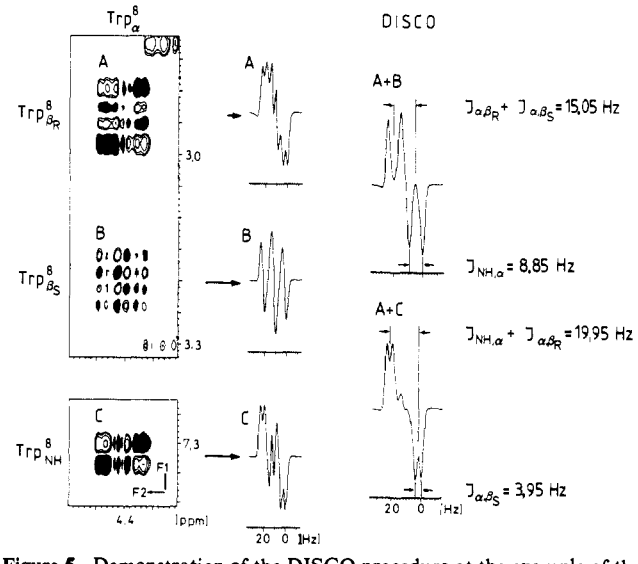

Figure 5. Demonstration of the DISCO procedure at the example of the cross peaks of $TrpH^{\beta pro\text{-}R}$, $H^{\beta pro\text{-}S}$, and NH to the α proton. Three pseudo-1D spectra are obtained after coaddition. Weighted combination of A + B and A + C yields simplified patterns from which the $J(H^{\alpha},H^{\beta pro\text{-}R})$, $J(H^{\alpha},H^{\beta pro\text{-}S})$, and $J(NH,H_{\alpha})$ coupling constants are obtained.

implies, for example, that NH,H^{α} coupling constants can be extracted from amino acids with two β protons. The weighting factor for the combination of those pseudo-1D spectra is unknown and must be determined from the result of the combination by inspection. This is easily done when only a few couplings are present in a multiplet, but is very difficult or impossible for larger spin systems such as proline, where only the E.COSY spectrum gave access to the coupling constants. Strong coupling effects in addition may prevent finding the proper weighting. Systematic errors due to partial overlap of antiphase signals should also be recognized as a possible objection to DISCO.

In contrast to the data manipulation procedure DISCO, E. COSY is a pulse technique. It requires phase increments smaller than 90°. E.COSY simplifies cross-peak multiplets the more efficiently the more "relevant"[51] coupling constants are found in the cross peak. E.COSY therefore is especially suited for complicated spin systems, although it already simplifies cross peaks of three mutually coupled spins. Those simplified cross-peak patterns are easily analyzed by inspection. In addition, relative signs of coupling constants are accessible and coupling constants as small as one-tenth of the line width can be determined.[52] Strong coupling is tolerated to a large extent. The evaluation of E.COSY spectra involves coaddition only over parts of the cross peak. This results in a lower signal-to-noise ratio of the pseudo-1D spectra compared to the DISCO spectra.

Table VII. Coupling Constants of the D-Pro^1 Residue of **1** Obtained from the E.COSY Spectrum

J(H,H)	Hz	J(H,H)	Hz
$H^{\alpha},H^{\beta pro\text{-}R}$	7.8	H^{γ},H^{γ}	−11.7
$H^{\alpha},H^{\beta pro\text{-}S}$	5.2	$H^{\gamma pro\text{-}S},H^{\delta pro\text{-}R}$	7.0
H^{β},H^{β}	−12.4	$H^{\gamma pro\text{-}S},H^{\delta pro\text{-}S}$	6.7
$H^{\beta pro\text{-}R},H^{\gamma pro\text{-}S}$	7.5	$H^{\gamma pro\text{-}R},H^{\delta pro\text{-}R}$	6.0
$H^{\beta pro\text{-}R},H^{\gamma pro\text{-}R}$	6.3	$H^{\gamma pro\text{-}R},H^{\delta pro\text{-}S}$	6.7
$H^{\beta pro\text{-}S},H^{\gamma pro\text{-}S}$	7.0	H^{δ},H^{δ}	−10.5
$H^{\beta pro\text{-}S},H^{\gamma pro\text{-}R}$	6.1		

The Thr^3 H^{α},H^{β} coupling constant is determined at the Thr$^3H^{\alpha}$ resonance in the one-dimensional spectrum of the Phe^6 deuterated derivative **4**. Also a z-filtered 1D-COSY spectrum[53] using Gaussian pulses[54] applied to the NH signal of Thr in the non-deuterated peptide yields the identical information (see supplementary material). The vicinal and geminal coupling constants of the D-Pro^1 residue could be determined from the E.COSY spectrum (see supplementary material) in spite of quite strong coupling (Table VII). The degeneracy of the Lys β protons prevent the extraction of the individual H^{α},H^{β} coupling constants in this residue.

For the determination of proton–proton distances a ROESY experiment was performed using small flip angles (17°) instead of 180° pulses for the mixing sequence to suppress contributions

(53) Kessler, H.; Bermel, W.; Griesinger, C.; Oschkinat, H. *J. Magn. Reson.* **1986**, *70*, 106–133.
(54) Bauer, C.; Freeman, R.; Frenkiel, T.; Keeler, J.; Shaka, A. J. *J. Magn. Reson.* **1984**, *58*, 442–457.

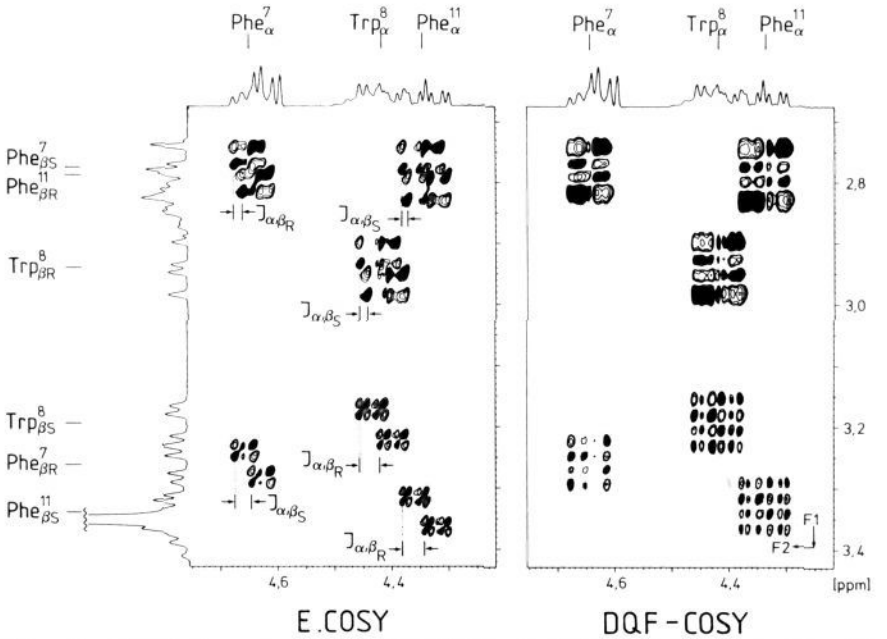

Figure 6. Comparison of the section of the (α,β) cross peaks obtained by E.COSY and a DQF-COSY. Positive signal intensities are indicated as filled contours. The extraction procedure for coupling constants is indicated. The displacement vectors of the basic rectangular pattern contain in the F2 dimension the coupling of the passive spin to the spin active in F2. For instance, the Phe^{6}H$^{\beta pro\text{-}R}$-Phe^{6}H$^\alpha$ cross peak provides the Phe^{6}H$^{\beta pro\text{-}S}$–Phe^{6}H$^\alpha$ coupling.

from J coupling.[39] The quantitative evaluation starts with volume integration. Offsets of the base plane are corrected. Relative rotating frame NOE's are thus obtained. Assuming linearity of the integrals in the ROESY experiment and rotating from cross-relaxation rates and a zero laboratory frame NOE (which is experimentally checked), the offset dependence of the ROE's can be taken into account in the formula for the distance r_{ij} between the spins i and j,[37,40] where I_{ij} is the integral of the ROE cross peak. β_i is defined as

$$r_{ij} \approx \left\{ \frac{\sin^2 \beta_i \sin^2 \beta_j}{I_{ij}} \right\}^{1/6} \qquad \beta_i = \arctan \frac{\gamma B_1}{\Omega_i}$$

B_1 is the field strength of the locking field and Ω_i is the resonance offset of the nucleus i.

The ROE's are calibrated with respect to the ROE value of the indole NH proton to the H′$_7$ proton and the known distance NH–H′$_7$ = 282 pm.[55] The relaxation times of the indole carbons (Figure 11) indicate similar flexibility of the indole ring and the rest of the molecule, which is essential for calibration (Table VIII). *Independent proof of the correctness of this calibration is given* by the cross-peak intensities between geminal protons, for example, D-Pro^1-H$^\delta$/H$^\delta$ = 178 pm, which is in agreement with the known distance.

The T_1 relaxation times of the ^{13}C resonances are determined by the inversion-recovery technique.[56,57] The measurements were done separately for the aliphatic carbon and for the aromatic and the carbonyl resonances. The NOE enhancements are far from 2 for the aliphatic carbons. This is expected for a molecule which shows no proton–proton NOE's in the laboratory frame and thus has a correlation time of about 0.5 ns ($\omega_0\tau_c \approx \sqrt{5}/2$). The carbons in the side chains show the full enhancement in agreement with their increased mobility. The relaxation rates are given by:[58]

$$\frac{1}{NT_1} = \frac{3}{20} \frac{\gamma_H^2 \gamma_C^2 \hbar^2}{r^6} \frac{\tau_c}{1 + \omega^2(^{13}C)\tau_c^2}$$

Table VIII. Proton–Proton Distances Obtained from the ROESY Spectrum of **1**[a]

No.	involved protons		distance [pm]	No.	involved protons		distance [pm]
1.	D-Pro^{1}H$^\alpha$	D-Pro^{1}H$^{\beta pro\text{-}R}$	219	26.	Trp^{5}NH	Lys^{4}H$^\alpha$	262
2.	D-Pro^{1}H$^\alpha$	D-Pro^{1}H$^{\beta pro\text{-}S}$	270	27.	Trp^{5}NH	Lys^{4}H$^\beta$	313
3.	D-Pro^{1}H$^{\gamma pro\text{-}R}$	D-Pro^{1}H$^{\delta pro\text{-}S}$	245	28.	Trp^{5}NH	Trp^{5}H$^{\beta pro\text{-}R}$	260
4.	D-Pro^{1}H$^{\gamma pro\text{-}S}$	D-Pro^{1}H$^{\delta pro\text{-}R}$	255	29.	Trp^{5}NH	Trp^{5}H$^{\beta pro\text{-}S}$	315
5.	Phe^{2}NH	D-Pro^{1}H$^\alpha$	196	30.	Trp^{5}H$^1_2$	Trp^{5}H$^{\beta pro\text{-}R}$	264
6.	Phe^{2}NH	Phe^{2}H$^\alpha$	263	31.	Trp^{5}H$^1_2$	Trp^{5}H$^{\beta pro\text{-}S}$	269
7.	Phe^{2}NH	Phe^{2}H$^{\beta pro\text{-}R}$	240	32.	Trp^{5}H$^1_4$	Trp^{5}H$^\alpha$	257
8.	Phe^{2}NH	Thr^{3}NH	267	33.	Trp^{5}H$^1_4$	Trp^{5}H$^{\beta pro\text{-}S}$	305
9.	Phe^{2}H$^{\beta pro\text{-}S}$	Thr^{3}H$^\gamma$	257	34.	Trp^{5}H$^1_4$	Trp^{5}H$^{\beta pro\text{-}R}$	298
10.	Thr^{3}NH	Phe^{2}H$^\alpha$	265	35.	Trp^{5}H$^1_4$	Lys^{4}H$^\beta$	360
11.	Thr^{3}NH	Thr^{3}H$^\alpha$	265	36.	Phe^{6}NH	Thr^{3}OH	284
12.	Thr^{3}NH	Thr^{3}H$^\beta$	339	37.	Phe^{6}NH	Lys^{4}H$^\beta$	319
13.	Thr^{3}NH	Thr^{3}H$^\gamma$	268	38.	Phe^{6}NH	Phe^{6}H$^\alpha$	282
14.	Thr^{3}NH	Thr^{3}OH	321	39.	Phe^{6}NH	Phe^{6}H$^{\beta pro\text{-}S}$	269
15.	Thr^{3}H$^\gamma$	Thr^{3}H$^\alpha$	245	40.	Phe^{6}NH	Phe^{6}H$^{\beta pro\text{-}R}$	332
16.	Thr^{3}H$^\gamma$	Thr^{3}H$^\beta$	219	41.	Phe^{6}H$^\alpha$	D-Pro^{1}H$^{\delta pro\text{-}S}$	221
17.	Thr^{3}H$^\gamma$	Thr^{3}OH	288	42.	Phe^{6}H$^\alpha$	D-Pro^{1}H$^{\delta pro\text{-}R}$	217
18.	Lys^{4}NH	Thr^{3}H$^\alpha$	228	43.	Phe^{6}H$^\alpha$	D-Pro^{1}H$^\alpha$	267
19.	Lys^{4}NH	Thr^{3}H$^\beta$	223	44.	Phe^{6}H$^\alpha$	D-Pro^{1}H$^{\delta pro\text{-}S}$	325
20.	Lys^{4}NH	Lys^{4}H$^\alpha$	265	45.	Phe^{6}H$^\alpha$	Lys^{4}H$^\beta$	341
21.	Lys^{4}NH	Lys^{4}H$^\beta$	251	46.	Phe^{6}H$^\alpha$	Phe^{6}H$^\alpha$	258
22.	Lys^{4}NH	Lys^{4}H$^\gamma$	291	47.	Phe^{6}H$^\alpha$	Phe^{6}H$^{\beta pro\text{-}R}$	248
23.	Lys^{4}NH	Trp^{5}NH	311	48.	Phe^{6}H^m	D-Pro^{1}H$^\alpha$	313
24.	Lys^{4}H$^\gamma$	Lys^{4}H$^\alpha$	253	49.	Phe^{6}H^m	D-Pro^{1}H$^{\delta pro\text{-}S}$	350
25.	Lys^{4}H$^\gamma$	Lys^{4}H$^\epsilon$	258	50.	Phe^{6}H^m	Phe^{6}H$^\alpha$	339

[a] Recorded at 300-MHz spectrometer frequency in Me_2SO Solution at 300 K: mixing time, 0.2 s; flip angle, 17°; B_1 field strength, 1.7 kHz.

Still, the dipolar relaxation rates $1/NT_1$ of the carbons depend linearly on the τ_c values because the $1 + (\omega(^{13}C)\tau_c)^2$ denominator varies only between 1 and 1.06 for the whole range of τ_c values for this molecule: (τ_c = 0 to 0.5 ns). The relaxation can safely be assumed to occur exclusively due to H,C dipolar coupling for such molecules. There is no measurable external relaxation, since the very mobile groups in the molecule show the full NOE (aromatic protons, methyl groups). Spin rotation relaxation is obviously absent since methyl groups show the full NOE en-

(55) Bye, E.; Mostad, A.; Rømming, C. *Acta Chem. Scand.* **1973**, *27*, 471–484.
(56) Vold, R. L.; Waugh, J. S.; Klein, M. P.; Phelps, D. E. *J. Chem. Phys.* **1968**, *48*, 3831.
(57) Deslauriers, R.; Smith, I. C. P. *Top. Carbon-13 NMR Spectrosc.* **1976**, *2*, 1–80.
(58) Noggle, J. H.; Shirmer, R. E. *The Nuclear Overhauser Effect*; Academic Press: New York, 1971.

Table IX. Temperature Dependence of the NH Chemical Shifts in $-\Delta\delta/\Delta T$ (ppb/K) and Scaling Factors of the MD Calculation ii

	Phe^2	Thr^3	Lys^4	Trp^5	Phe^6
$-\Delta\delta/\Delta T$	7.0	3.3	4.3	3.0	1.0
factor	0.25	0.71	0.59	0.75	1.0

Table X. Hydrogen Bonds[a] in **1** Averaged during 50-ps Molecular Dynamics Calculations. Comparison of the Values of Calculations i and ii (italics)

		r(H–A)[b] (pm)		θ[c] (deg)		population (%)	
donor	acceptor	i	ii	i	ii	i	ii
Thr^{3}NH	D-Pro^{1}CO	215	*229*	138	*133*	59	*25*
Thr^{3}NH	Phe^{6}CO	218	*216*	147	*151*	56	*84*
Thr^{3}OH	Phe^{6}CO	197	*201*	140	*140*	54	*37*
Trp^{5}NH	Thr^{3}OH	272	*271*	147	*144*	52	*42*
Trp^{5}NH	Thr^{3}CO	195		145		22	
Phe^{6}NH	Thr^{3}OH	232	*236*	148	*144*	91	*87*
Phe^{6}NH	Thr^{3}CO	229	*225*	139	*139*	39	*63*

[a] Definition of hydrogen bridges: D–H A is shorter than 300 pm and the corresponding θ angle is greater than 120°. [b] Distance between X*H*-donor and Y-acceptor. [c] Angle between (D–H A).

hancement. Relaxation due to chemical shift anisotropy can be calculated with formulas in ref 59 and 60 for our molecule ($\tau_c \approx 0.5$ ns, $\gamma_H B_1/\hbar = 300$ MHz, and $\delta_Z < 200$ ppm) to be irrelevant, too.

Backbone Conformation

The spectrum of **1** contains only one set of signals. Thus there is no detectable conformational equilibrium involving a barrier of more than 60 kJ/mol, i.e., cis–trans isomerism about the Phe^6-D-Pro^1 amide bond. Fast interconverting conformations cannot be excluded from this finding. In fact, it is very difficult to decide whether a molecule is conformationally homogeneous or not.[17] This can only be done at the end of the conformational analysis, possibly with computer assistance, when the assumption of one predominant conformation does not contradict the data. Fortunately, there are some empirical rules which when fulfilled usually, but not always, indicate conformational homogeneity.[14,15,17] They are fulfilled by **1**.

The characteristic chemical shift of the D-Pro^1 C^β and C^γ resonances (H,C-COSY spectrum; see supplementary material) reveal a trans Phe^6-D-Pro^1 peptide bond.[17,61,62] The temperature dependence of the NH chemical shifts (Table IX) indicates the Phe^2-NH to be oriented externally, because of the large $-\Delta\delta/\Delta T$ coefficient. The small cofficient of the Phe^6-NH suggests that this proton is involved in an intramolecular hydrogen bond. The other temperature coefficients cannot be interpreted conclusively at this stage, because they lie in an intermediate range.[17,63]

Taking into account the characteristic $C^\alpha H^{i-1}NH^i$ NOE effects, a βI,βII′ structure is derived for this peptide with Thr^3-CO-NH-Phe^6 and Phe^6-CO-NH-Thr^3 hydrogen bridges.[10,64] As we will see later on, the βII′ turn is well represented in the MD calculation, but in addition a γ^i turn is suggested involving the NH of Thr^3 and the CO group of D-Pro^1. However, the hydrogen bridges in the βI turn region are differently interpreted by the MD calculations (see below). It must be pointed out, that NH,H$^\alpha$ homonuclear coupling constants are in agreement with both conformational proposals. This will be discussed below. A βI turn involving the Thr^{3}CO is in excellent agreement with the relatively small ^3J(NH,H$^\alpha$) coupling constant of Lys^4 (predicted $\varphi = -60°$, corresponding to 3.4 Hz) and a large value of Trp^5 (predicted $\varphi = -90°$, corresponding to 8.9 Hz). The small Trp^5 NH,H$^\alpha$ cross peak in the ROESY spectrum recorded with small mixing pulses (only a semiquantitative evaluation is possible because the cross peak lies in a crowded region; see Table III), the cross peak between the Trp^{5}NH and Lys^{4}H$^\beta$ protons (these protons are oriented above the backbone), and the missing Lys^{4}C′-Trp^{5}H$^\alpha$ cross peak in the H,C-COLOC spectrum of **1**[68] (which exclude an antiperiplanar orientation of the Lys^{4}C′ and Trp^{5}H$^\alpha$ nuclei) are indicators for a βI turn. In the βII′ region the coupling constant ^3J(NH,H$^\alpha$) of Phe^2 ($\varphi = -100°$) allows a βI or βII′ turn; however, a βI turn is excluded in this region by the NOE effect between Phe^{2}NH and Thr^{3}NH. In addition, the strong NOE effect between D-Pro^{1}H$^\alpha$ and Phe^{2}NH supports the βII′ turn, and the small NOE effect between Thr^{3}NH and Phe^{2}H$^\alpha$ reflects the long distance between these protons in a βII′ turn.

Side-Chain Conformation

Generally, side chains are more flexible than the backbone, and conformational homogeneity is not expected. The most important conformational parameter for the side-chain conformation is the torsional angle χ_1 about the C^α–C^β bond. The population of the three staggered conformations ($\chi_1 = 60°, -60°, 180°$) is determined from vicinal ^3J(H$^\alpha$,H$^\beta$) coupling constants using Pachler's equations.[65-67] The assignment of the diastereotopic β protons, necessary for the distinction between $\chi_1 = -60$ and 180°, has been derived from the stereoselectively deuterated compounds (Table VI).

Another approach which relies on heteronuclear coupling constants of the nondeuterated compound is described elsewhere.[68-70] The results thus obtained are identical with those obtained from the deuterated compounds. Table VI lists the populations of the side chains. The main result is that Phe^2 and Trp^5 prefer conformation I, whereas Phe^6 populates predominantly conformation II. The orientation of the Phe^6 side chain is supported by the ROE cross peaks between aromatic ortho and meta protons of Phe^6 to the D-Pro^1 protons: H^o–H$^\alpha$, H^o–H$^{\delta pro\text{-}S}$, H^m–H$^\alpha$, and H^m–H$^{\delta pro\text{-}S}$. A small H$^\alpha$,H$^\beta$ coupling constant is obtained for Thr^3 (3.5 Hz). A strong Lys^{4}NH-Thr^{3}H$^\beta$ cross peak in the NOESY and ROESY spectrum, as well as a missing Thr^{3}H$^\beta$-C′ cross peak in the H,C-COLOC[69] spectrum, indicates the predominance of conformation I (Table VI). The coupling constants in the proline ring suggest a flexible conformation.[71-75] The stereochemical assignment of the β protons is achieved by the strong NOE effect between H$^\alpha$ and H$^{\beta pro\text{-}R}$ (500-MHz NOESY spectrum). The assignment of all other protons in the proline ring then follows from the vicinal coupling constants.

Chemical shift effects in peptides are often difficult to explain. However, anisotropy effects from carbonyl groups and/or aromatic side chains may provide additional conformational information. With the assignment of the diastereotopic β protons of the aromatic amino acids and proline, we can discuss their chemical shifts with respect to the conformation. For example, the H$^{\beta pro\text{-}R}$ proton of Phe^6 is close to the CO of the Trp^5 residue. Accordingly, we

(59) Mehring, M. *Principles of High Resolution NMR in Solids*, 2nd ed.; Springer Verlag: Berlin, 1983.
(60) Abragam, A. *Principles of Nuclear Magnetism*; Clarendon Press: Oxford, 1985.
(61) Deber, C. M.; Madison, V.; Blout, E. R. *Acc. Chem. Res.* **1976**, *9*, 106.
(62) Siemion, I. Z.; Wieland, T.; Pook, K. H. *Angew. Chem., Int. Ed. Engl.* **1975**, *14*, 702.
(63) Ovchinnikov, Y.; Ivanov, V. T. *Tetrahedron* **1975**, *31*, 2177–2209.
(64) Kessler, H.; Gehrke, M.; Haupt, A.; Klein, M.; Müller, A.; Wagner, K. *Klin. Wochenschr.* **1986**, *64*, 74–78.
(65) Pachler, K. G. R. *Spectrochim. Acta* **1963**, *19*, 2085–2092.
(66) Pachler, K. G. R. *Spectrochim. Acta* **1964**, *20*, 581–587.
(67) Bystrov, V. F. *Progr. NMR Spectrosc.* **1976**, *10*, 41–82.
(68) Griesinger, C. "Entwicklung neuer NMR spektroskopischer Methoden, Konformationsanalyse zyklischer Peptide"; Ph.D. Thesis, Frankfurt, Germany, 1986.
(69) Kessler, H.; Griesinger, C.; Wagner, K. *J. Am. Chem. Soc.* **1987**, *109*, 6927–6933.
(70) Anders, U.; Gemmecker, G.; Kessler, H.; Griesinger, C. *Fresenius Z. Anal. Chem.* **1987**, *327*, 72–73.
(71) Kopple, K. D.; Wiley, G. R.; Tauke, R. *Biopolymers* **1973**, *12*, 627.
(72) Haasnoot, F. C. A. G.; de Leeuw, F. A. A. M.; de Leeuw, H. P. M.; Altona, C. *Biopolymers* **1981**, *20*, 1211.
(73) Haasnoot, F. C. A. G.; de Leeuw, F. A. A. M.; Altona, C. *Tetrahedron* **1980**, *36*, 2783–2792.
(74) Kessler, H.; Bermel.; Friedrich, A.; Krack, G.; Hull, W. E. *J. Am. Chem. Soc.* **1982**, *104*, 6297–6304.
(75) de Leeuw, F. A. A. M.; Altona, C.; Kessler, H.; Bermel, W.; Friedrich, A.; Krack, G.; Hull, W. E. *J. Am. Chem. Soc.* **1983**, *105*, 2237–2246.

Table XI. Comparison of the Backbone Angles Averaged during 50-ps Molecular Dynamics Calculations (i and ii) and the Experimental Values

	^3J(NH,H$^\alpha$) (Hz)	φ^{exptl} (deg)	φ^{MD} (deg)	$\varphi^{MD-exptl}$ (deg)	ψ^{MD} (deg)	ω^{MD} (deg)
D-Pro^1			59 (10)[a]		−104 (11)[b]	178 (6)
			61 (10)		*−105 (10)*	*177 (6)*
Phe^2	8.9	−100	−68 (15)	32	0 (23)	−177 (8)
			−65 (14)	*35*	*−15 (22)*	*179 (8)*
Thr^3	9.7	−130	−137 (17)	7	164 (10)	177 (7)
			−119 (20)	*11*	*162 (9)*	*178 (7)*
Lys^4	3.4	−62	−51 (16)	11	−22 (28)	−178 (7)
			−46 (13)	*16*	*−37 (18)*	*−179 (6)*
Trp^5	8.9	−100	−108 (27)	8	−41 (15)	−178 (7)
			−96 (20)	*4*	*−34 (15)*	*−176 (7)*
Phe^6	5.8	−160	−142 (19)	18	111 (15)	172 (7)
			−145 (16)	*15*	*107 (14)*	*172 (7)*

[a] First entry, calculation i; second entry, calculation ii. [b] Values in parentheses: RMSF.

observe a downfield shift of this resonance. The $H^{\beta pro\text{-}R}$ proton of Trp^5 and the $H^{\beta pro\text{-}S}$ proton of Phe^2 approach the carbonyl group of the same amino acid and therefore also resonate downfield with respect to their diastereotopic counterpart. The preferred conformation II of the Phe^6 side chain in connection with the orientation of the aromatic ring over the D-Pro^1 ring gives rise to a strong high-field shift of the $H^{\delta pro\text{-}S}$ proton of D-Pro^1 to 2.52 ppm. Hence, in our case the observed chemical shifts of some protons are in agreement with the proposed conformation. The predominant conformation of **1** is shown in Figure 7.

Refinement of the Conformation by Molecular Dynamics Calculations

The limited possibilities to include all nuclear distances and the lack of energetic information in classical modelling by mechanical models such as Dreiding or "FMM" models led us to the application of computer-assisted modelling (see Experimental Section). For this purpose the GROMOS program[76,77] (*GRO*ningen *MO*lecular *S*imulation Package) was used. The GROMOS force field has been developed for application to aqueous or apolar solutions of proteins, nucleotides, and sugars. However, a version suitable for simulations in vacuo is also available.[1,77-83] In order to account for the influence of the solvent on the conformation of the solute, experimental distance constraints were included in the simulations. To our experience, the MD calculations in vacuo tend to overestimate the presence of γ turns. We consider the origin of this effect to be the overemphasized electrostatic interactions because in reality charges are shielded by solvation. We therefore performed two independent MD calculations using 31 experimental distances as constraints: (i) common GROMOS force field and (ii) the same force field but using reduced charges at solvent exposed NH hydrogens. Experimental temperature gradients of the NH protons are used to calculate the effective charges: no reduction of the charge was done for Phe^{6}NH ($-\Delta\delta/\Delta T$ = 1.0 ppb/K), whereas a maximum reduction by 75% was fixed for Phe^{2}NH ($-\Delta\delta/\Delta T$ = 7.0 ppb/K). The effective charges of the other NH's were obtained from linear interpolation. An unsymmetrical ROE constraint pseudopotential was used to take into account the tendency to overestimate short distances due to the r^{-6} dependence of ROEs in case of flexible systems (see Experimental Section). The resulting conformations (i and ii) are shown in Figure 8 and results are given in Tables XI–XIII.

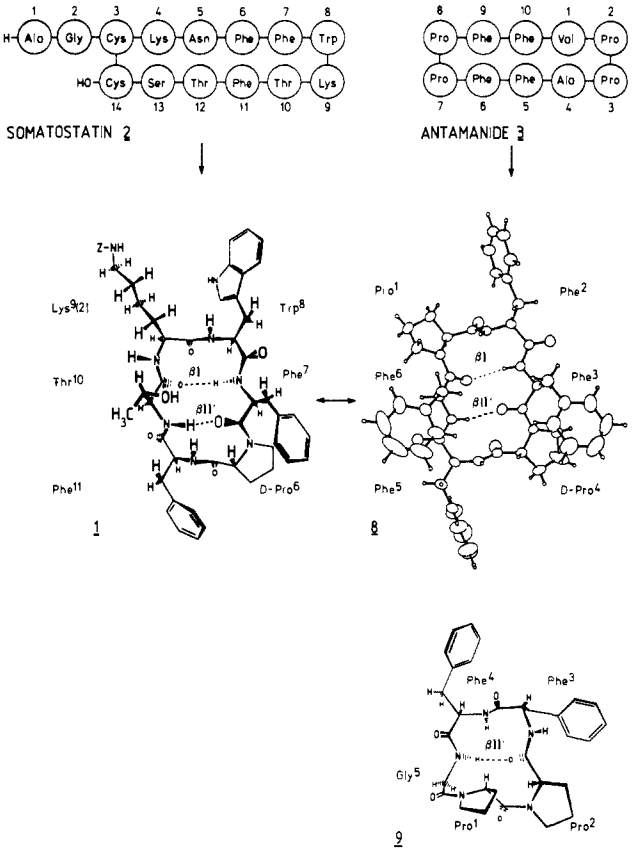

Figure 7. Cyclic peptides with high cytoprotective potency. Compound **1** was derived from somatostatin; **8** uses two Phe-Phe-Pro building blocks of **3**. The constitutions of **1** and **8**, however, are very similar. The comparison of the solution structure of **1** and the solid-state conformation of **8** shows close similarity. The cyclic pentapeptide **9** (on the bottom) adopts a different spatial structure and is inactive in the biological test although it contains sequence homology (-Pro-Pro-Phe-Phe-) to **3**.

The experimental data of the NMR measurements, NOE's and J couplings, are well represented in the calculations (Table XI–XIII). Both calculated conformations exhibit a βII′ turn about D-Pro^1-Phe^2 and to a lesser extent a βI turn about Lys^4-Trp^5. In contrast to the originally proposed conformation a *bifurcated* hydrogen bond[84] of the Thr^3-NH to the D-Pro^1-CO forming an additional γ^i turn is found in calculation i (population: 59%) but as expected the occurrence of this γ^i turn is drastically reduced in calculation ii (population: 25%). A similar observation is made in the *upper part* (Thr^3-Lys^4-Trp^5-Phe^6). The Thr^3-CO group accepts only the Phe^{6}NH establishing a βI turn (population: 63%) in calculation ii. However, the population of the βI turn is reduced in the conventional calculation i (population: 39%), and a γ^i turn

(76) Åquist, J.; van Gunsteren, W. F.; Leijonmark, M.; Tupia, O. *J. Mol. Biol.* **1985**, *183*, 461–477.
(77) van Gunsteren, W. F.; Kaptein, R.; Zuiderweg, E. R. P. *Nucleic Acid Conformation and Dynamics*; Olsen, W. K., Eds.; 1983, pp 79–92.
(78) Kaptein, R.; Zuiderweg, E. R. P.; Scheek, R. M.; van Gunsteren, W. F. *J. Mol. Biol.* **1985**, *182*, 179–182.
(79) Nilsson, L.; Clore, G. M.; Gronenborn, A. M.; Brünger, A. T.; Karplus, M. *J. Mol. Biol.* **1986**, *188*, 455–475.
(80) Clore, G. M.; Gronenborn, A. M.; Brünger, A. T.; Karplus, M. *J. Mol. Biol.* **1985**, *186*, 435–455.
(81) Lautz, J.; Kessler, H.; Kaptein, R.; van Gunsteren, W. F. *J. Computer Aided, Mol. Design*, in press.
(82) van Gunsteren, W. F.; Boelens, R.; Kaptein, R.; Scheck, R. M.; Zuiderweg, E. R. P. *Molecular Dynamics and Protein Structure*; Hermans, H., Ed.; Polycrystal Book Service: Western Springs, IL, 1985; pp 92–99.
(83) Weiner, S. J.; Kollman, P.; Case, D. A.; Singh, U. C.; Ghio, C.; Alagona, G.; Profeta, S.; Weiner, P. *J. Am. Chem. Soc.* **1984**, *106*, 765–784.
(84) Sänger, W. *Annu. Rev. Biophys. Biophys. Chem.* **1987**, *16*, 93–114.

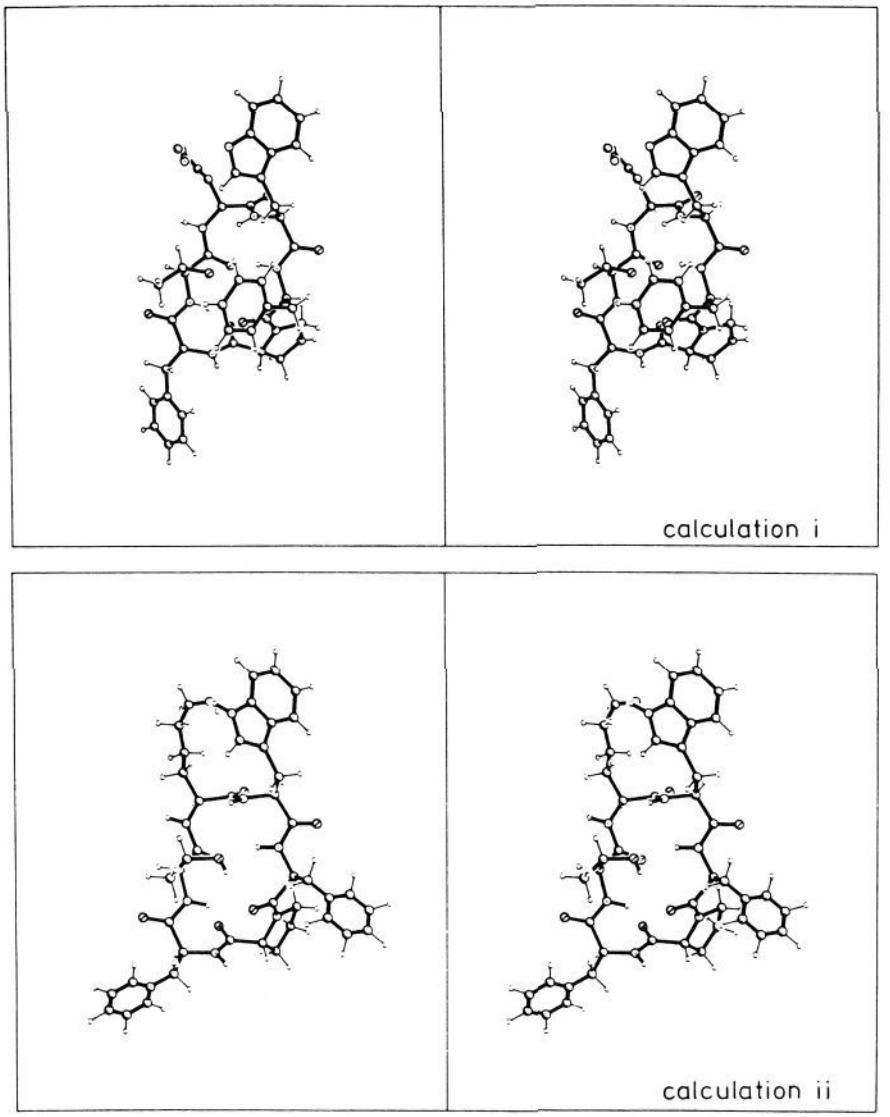

Figure 8. Mean conformation of *cyclo*(-D-Pro-Phe-Thr-Lys(Z)-Trp-Phe-) (**1**) obtained by 50-ps restraint MD calculation i (upper) and ii (minor) in vacuo. The protons of the Lys residue are not shown in calculation i because of the large fluctuation of the Lys side chain during the MD run.

between Thr^3-CO and Trp^5-NH (22%) is formed in addition. Thus, the inclusion of the experimentally observed temperature gradients to reduce charge effects leads to a conformation which is closer to the originally proposed structure[10] and resembles to a large extent the backbone conformation of analogue **7** in the crystal (see below).

The main difference in the X-ray structure of **7** is found in the orientation of the Thr^3 side chain. Its hydroxyl group accepts hydrogen bridges from the two NH protons of Trp^5 and Phe^6 but also forms a donor hydrogen bridge to the carbonyl oxygen of Phe^6. A spacefilling drawing (Figure 9) shows a compact packing of the Thr-OH in the center of the molecule. The influence of the Thr-OH group on the backbone conformation is expressed comparing a derivative of **1** in which the Thr is substituted by Val.[85,86] In this analogue, *cyclo*(-D-Pro-Phe-Val-Lys(Z)-Trp-Phe-), the Lys-Trp peptide bond is rotated by 180°. Thus, a βII turn is formed instead of a βI turn.

Although "ROE distances" to the stereospecifically assigned β protons of the aromatic amino acids are included in the calculations, the mean orientation of Phe^2 ($\chi_1 = 141°$ in calculation ii) deviates significantly from the $\chi_1 = -60°$ (I) as derived from the coupling constants (see above). Obviously the ROE constraints

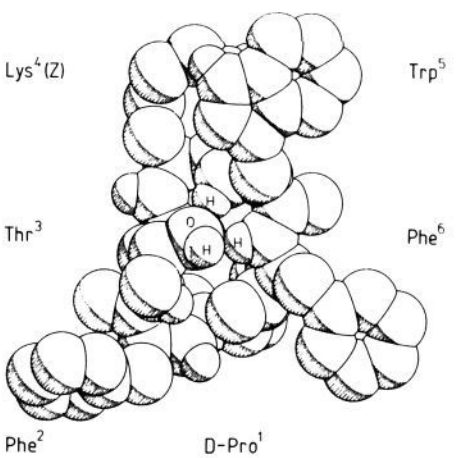

Figure 9. Same as Figure 8, calculation ii, a space-filling drawing. It shows the hydrogen bonding of the Thr-OH group. The hydroxyl group is responsible for the compact packing of **1**.

alone are not sufficient to find the most populated conformation. In calculation i a mean value $\chi_1 = -74°$ is found although the distance Phe^2NH to $Phe^2H^{\beta pro\text{-}R}$ is identical in both calculations (Table XII). In a free dynamic calculation side-chain rotations

(85) Haupt, A. Ph.D. Thesis, Frankfurt, Germany, 1987.
(86) Wagner, K. Ph.D. Thesis, Frankfurt, Germany, 1988.

Table XII. Comparison of Experimental and Calculated Proton–Proton Distances [pm] Obtained from the ROESY Experiment and the Molecular Dynamic Calculations

No	involved protons		$r(H,H)^{exp}$	$r(H,H)^{MDi}$	$r(H,H)^{MDii}$
1.	Phe^2NH	- $D\text{-}Pro^1H^\alpha$	196[a]	206	205
2.	Phe^2NH	- Phe^2H^α	263	271	272
3.	Phe^2NH	- $Phe^2H^{\beta pro\text{-}R}$	240	230	231
4.	Phe^2NH	- Thr^3NH	267	294	278
5.	$Phe^2H^{\beta pro\text{-}S}$	- Thr^3H^γ	257 - 357[b]	447	419
6.	Thr^3NH	- Phe^2H^α	265	301	319
7.	Thr^3NH	- Thr^3H^α	265	279	282
8.	Thr^3NH	- Thr^3H^β	339	382	373
9.	Thr^3NH	- Thr^3H^γ	268 - 368	391	366
10.	Thr^3NH	- Thr^3OH	321	300	298
11.	Thr^3OH	- Phe^6NH	284	268	280
12.	Thr^3OH	- Thr^3N^γ	288 - 388	276	273
13.	Thr^3H^α	- Thr^3H^γ	245 - 345	294	295
14.	Lys^4NH	- Trp^5NH	311	308	303
15.	Lys^4NH	- Thr^3H^α	228	243	242
16.	Lys^4NH	- Thr^3H^β	223	249	250
17.	Lys^4NH	- Lys^4H^α	265	261	261
18.	Lys^4NH	- Lys^4H^β	251 - 341	262	231
19.	Lys^4NH	- Lys^4H^γ	291 - 381	336	404
20.	Lys^4H^α	- Lys^4H^γ	253 - 343	269	270
21.	Trp^5NH	- Lys^4H^α	262	320	334
22.	Trp^5NH	- Lys^4H^β	313 - 403	335	316
23.	Trp^5NH	- $Trp^5H^{\beta pro\text{-}S}$	315	361	354
24.	Trp^5NH	- $Trp^5H^{\beta pro\text{-}R}$	260	266	251
25.	$Trp^5H^\zeta_4$	- Trp^5H^α	257	282	283
26.	Phe^6NH	- Lys^4H^β	319 - 409	541	524
27.	Phe^6NH	- Phe^6H^α	282	278	279
28.	Phe^6NH	- $Phe^6H^{\beta pro\text{-}R}$	332	381	317
29.	Phe^6NH	- $Phe^6H^{\beta pro\text{-}S}$	269	332	311
30.	Phe^6H^α	- $D\text{-}Pro^1H^{\beta pro\text{-}S}$	221	219	224
31.	Phe^6H^α	- $D\text{-}Pro^1H^{\beta pro\text{-}R}$	217	236	235

[a] For the protons included in the united atoms virtuel positions were used.[83] [b] Pseudo-atom positions were used.[112]

are always found during a trajectory in the MD run. Calculations in vacuo also overemphasize the normally minor populated $\chi_1 = 60°$ conformation due to intramolecular interactions, e.g., without constraints Trp^5 always adopts this conformation. We therefore derive side-chain populations of C^α–C^β bond rotamers from J coupling only.

X-ray Structure Determination of the (Phe^4) Analogue of 1

Unfortunately it was not possible to obtain single crystals of **1** suitable for an X-ray structure determination. However, an analogue of **1** replacing the Lys^4 by a Phe residue was synthesized. Rather large single crystals of *cyclo*(-D-Pro-Phe-Thr-Phe-Trp-Phe-) (**7**) could be grown from saturated solution in acetone/methanol/water. Crystal structure determinations were performed for two different crystal modifications: an orthorhombic form containing one independent molecule and a monoclinic form containing two independent molecules (see Experimental Section). A perspective view containing the three molecules is shown in Figure 10.

The conformations of all three molecules are very similar and in close analogy to the conformation of **1** in solution. The backbone forms two β turns: type βII′ (about D-Pro^1-Phe^2) and type βI (about Phe^4-Trp^5). The observed backbone angles of the first one corresponds more closely to the typical angles for βII′ turns in peptides and proteins, whereas angles in the βI region deviate slightly from those. The orientation of the aromatic side chains Phe^2 and Trp^5 is surprisingly similar to that of the most stable side-chain conformation in solution: Phe^2 and Trp^5 adopt conformation I ($\chi_1 = -66$ to $-75°$, Table XVI) and in two of the three molecules Phe^6 prefers the conformation II ($\chi_1 = 173$ and 176°) as was found in solution. In the third molecule Phe^6 adopts an unusual conformation with a χ_1 value of 94°. This energetically unfavorable conformation with a large deviation from staggering is apparently a consequence of crystal packing effects. The presence of an acetone molecule in the crystal nearby excludes a χ_1 value of 180°. The side chain of Phe^4 is oriented perpendicular to the Trp^5 residue. This is a good example for the vertical staggering of aromatic residues, which are considered to provide additional binding. The main difference between the X-ray and the solution structure is the orientation of the Thr^3 side chain. As pointed out above, in solution the Thr-OH group binds *intramolecular* to two NH protons and the Phe^6 carbonyl oxygen. In the crystals, however, the hydroxyl group is involved in *intermolecular* hydrogen bonding to solvent molecules. Obviously,

Table XIII. Positional Parameters and Equivalent Values of Anisotropic Thermal Parameters of **7** (Orthorhombic Modification)

atom	x	y	z	B (Å^2)
O(Phe4)	−0.0299 (9)	−0.0260 (4)	0.4070 (3)	6.3 (2)
O(Trp5)	−0.115 (1)	−0.0285 (4)	0.2527 (3)	7.7 (2)
O(Phe6)	0.0984 (9)	0.1856 (4)	0.2841 (3)	6.2 (2)
O(Pro1)	0.446 (1)	0.1752 (4)	0.3380 (3)	6.2 (2)
O(Phe2)	0.236 (1)	0.3147 (5)	0.4501 (3)	7.7 (3)
O(Thr3)	0.083 (1)	0.1204 (4)	0.4009 (3)	6.4 (2)
O^γ(Thr3)	−0.241 (1)	0.2559 (4)	0.4459 (3)	6.6 (2)
N(Phe4)	−0.103 (1)	0.1272 (5)	0.4605 (4)	5.5 (3)
N(Trp5)	−0.212 (1)	0.0408 (4)	0.3799 (4)	4.6 (2)
N(Phe6)	−0.052 (1)	0.0687 (4)	0.2880 (4)	5.5 (3)
N(Pro1)	0.285 (1)	0.1347 (5)	0.2424 (3)	5.1 (2)
N(Phe2)	0.353 (1)	0.2731 (4)	0.3164 (3)	4.9 (2)
N(Thr3)	0.136 (1)	0.2472 (5)	0.3906 (4)	5.7 (3)
N-1(Trp5)	−0.726 (1)	−0.0192 (6)	0.3851 (4)	7.2 (3)
C′(Phe4)	−0.107 (1)	0.0212 (6)	0.4154 (5)	5.2 (3)
C^α(Phe4)	−0.105 (1)	0.0593 (5)	0.4676 (5)	5.1 (3)
C^β(Phe4)	−0.237 (2)	0.0422 (7)	0.5016 (5)	6.8 (4)
C-*i*(Phe4)	−0.244 (2)	−0.0300 (6)	0.5098 (5)	6.9 (4)
C-*o*1(Phe4)	−0.348 (2)	−0.0658 (7)	0.4820 (6)	9.3 (5)
C-*m*1(Phe4)	−0.355 (3)	−0.1317 (9)	0.4870 (6)	10.8 (6)
C-*p*(Phe4)	−0.247 (3)	−0.1647 (8)	0.5206 (7)	13.6 (7)
C-*m*2(Phe4)	−0.161 (3)	−0.1271 (9)	0.5491 (7)	14.9 (7)
C-*o*2(Phe4)	−0.152 (2)	−0.0630 (7)	0.5425 (6)	10.1 (5)
C′(Trp5)	−0.126 (1)	0.0138 (6)	0.2878 (5)	5.6 (3)
C^α(Trp5)	−0.233 (1)	0.0004 (6)	0.3341 (5)	4.8 (3)
C^β(Trp5)	−0.391 (1)	0.0128 (6)	0.3094 (5)	5.6 (3)
C-3(Trp5)	−0.514 (1)	−0.0161 (7)	0.3418 (5)	5.9 (3)
C-2(Trp5)	−0.628 (2)	0.0229 (6)	0.3592 (5)	6.4 (4)
C-7a(Trp5)	−0.680 (1)	−0.0822 (7)	0.3825 (5)	6.4 (4)
C-3a(Trp5)	−0.544 (1)	−0.0813 (5)	0.3564 (5)	4.9 (3)
C-4(Trp5)	−0.473 (2)	−0.1383 (6)	0.3474 (5)	5.8 (3)
C-5(Trp5)	−0.530 (2)	−0.1952 (8)	0.3662 (6)	8.1 (4)
C-6(Trp5)	−0.673 (2)	−0.1946 (7)	0.3912 (7)	9.7 (5)
C′(Phe6)	0.142 (1)	0.1383 (6)	0.2596 (4)	5.3 (3)
C^α(Phe6)	0.038 (1)	0.0844 (6)	0.2419 (5)	6.0 (3)
C^β(Phe6)	−0.057 (2)	0.1104 (7)	0.1969 (5)	6.8 (4)
C-*i*(Phe6)	0.026 (2)	0.1353 (8)	0.1507 (5)	7.3 (4)
C-*o*1(Phe6)	0.060 (2)	0.2011 (9)	0.1443 (6)	10.5 (5)
C-*m*1(Phe6)	0.138 (3)	0.226 (1)	0.1045 (7)	14.3 (7)
C-*p*(Phe6)	0.192 (2)	0.182 (1)	0.0698 (7)	15.6 (7)
C-*m*2(Phe6)	0.159 (2)	0.115 (1)	0.0704 (7)	12.6 (7)
C-*o*2(Phe6)	0.073 (2)	0.0903 (9)	0.1119 (6)	9.5 (5)
C′(Pro1)	0.396 (1)	0.2137 (5)	0.3056 (4)	4.8 (3)
C^α(Pro1)	0.377 (1)	0.1927 (6)	0.2492 (5)	5.6 (3)
C^β(Pro1)	0.526 (1)	0.1707 (7)	0.2258 (5)	6.6 (4)
C^γ(Pro1)	0.485 (2)	0.1175 (6)	0.1847 (6)	7.1 (4)
C^δ(Pro1)	0.357 (1)	0.0829 (6)	0.2117 (5)	5.7 (3)
C′(Phe2)	0.238 (2)	0.2874 (5)	0.4074 (5)	5.5 (3)
C^α(Phe2)	0.366 (1)	0.3028 (6)	0.3681 (5)	5.3 (3)
C^β(Phe2)	0.383 (2)	0.3763 (6)	0.3624 (5)	6.2 (3)
C-*i*(Phe2)	0.538 (2)	0.3940 (6)	0.3444 (5)	6.3 (4)
C-*o*1(Phe2)	0.647 (2)	0.4102 (6)	0.3836 (5)	7.3 (4)
C-*m*1(Phe2)	0.791 (2)	0.4241 (7)	0.3674 (7)	9.0 (5)
C-*p*(Phe2)	0.828 (2)	0.4226 (8)	0.3152 (7)	9.8 (5)
C-*m*2(Phe2)	0.723 (2)	0.4065 (7)	0.2776 (6)	8.5 (4)
C-*o*2(Phe2)	0.578 (2)	0.3940 (7)	0.2917 (5)	7.5 (4)
C′(Thr3)	−0.003 (2)	0.1551 (6)	0.4286 (5)	5.9 (3)
C^α(Thr3)	0.011 (1)	0.2279 (6)	0.4252 (5)	5.5 (3)
C^β(Thr3)	−0.131 (2)	0.2629 (6)	0.4053 (6)	7.0 (4)
C^γ(Thr3)	−0.185 (2)	0.2379 (7)	0.3522 (5)	7.2 (4)
C-7(Trp5)	−0.740 (2)	−0.1370 (7)	0.4000 (6)	9.3 (5)
H–O^γ(Thr3)	−0.2500	0.2988	0.4628	8
		Solvent		
O(W1)	−0.159 (1)	−0.1586 (5)	0.2547 (4)	8.6 (3)
O(W2)	−0.185 (1)	0.3628 (6)	0.5091 (4)	10.2 (3)
O(W3)	0.564 (1)	0.1495 (5)	0.4325 (4)	9.2 (3)

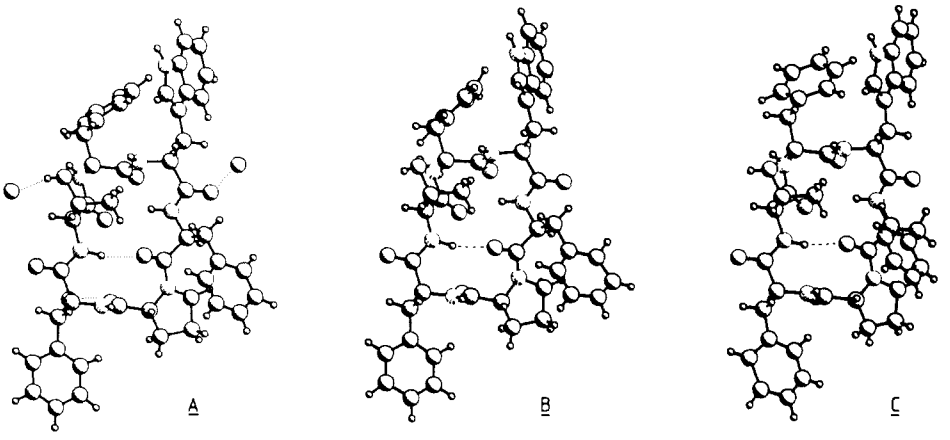

Figure 10. Perspective view of the three molecules in the crystal structure of **7**. (A) orthorhombic modification; (B) monoclinic modification, molecule 1; (C) monoclinic modification, molecule 2.

the association found in the crystal is disrupted in solution. Similar finding apply for cyclosporin A[87] where the OH group of the *N*-methylbutenylmethylthreonin (MeBmt) exhibits the same change upon dissolving the crystal. To our experience such differences between crystal and solution structure can always occur when intermolecular hydrogen bonds in the crystal stabilize the solid-state conformation.[87,88] In connection with the change of this side chain, a slight twist of the amide bond Lys[4]-Trp[5] is observed in solution. This conformational reorientation enables the NH proton of Trp[5] to approach the Thr-OH oxygen for hydrogen binding. Comparison of the conformation angles (Table XVI) found in the crystal structures for the three molecules shows that the molecules are quite rigid. Most rigid are the peptide bonds: the ω values do not vary significantly from one molecule to the other. Variations up to 15° are found for the φ and ψ values and seem to represent the molecular flexibility. The largest difference is found for residue Phe[6]. The reorientation of the side chain is found to have a considerable effect on the ψ value in the backbone. It changes by about 30°. The molecule has a βII′ turn between residues Thr[3] and Phe[6]. This bond is of intermediate strength and has similar dimensions in all three molecules (Thr[3]-NH→OC-Phe[6]: 3.00 (1), 2.98 (2), 2.95 (2) Å). In principle a second β turn can be formed between Phe[6]-NH and Thr[3]-CO. Only one of the three molecules contains such a bond and it is rather weak (Phe[6]NH→OC-Thr[3]: 3.14 (2) Å). In the other two molecules the observed NH→OC distance is too long for hydrogen bonding (3.29 (1) and 3.43 (2) Å). These findings resemble closely the observation of hydrogen bonding in solution.

Molecular Mobility

Experimental information about the molecular mobility can be obtained from the T_1 relaxation times of the carbon resonances,[89] as discussed above. The NT_1 values (N = number of attached protons, T_1 = longitudinal relaxation time) correlate directly with molecular mobility, when isotropic tumbling of the whole molecule and constant CH bond lengths are assumed.[90] The experimental data are given in Figure 11.

The α carbons all have very similar NT_1 values, indicating a "rigid" backbone. The mobility increases along the side chain of the Lys[4] residue showing that this side chain does not fold back to the backbone to build an intramolecular hydrogen bridge. The tendency to form intramolecular hydrogen bonds is reduced by the urethanic protecting group (Z).[91] The NT_1 values of the β

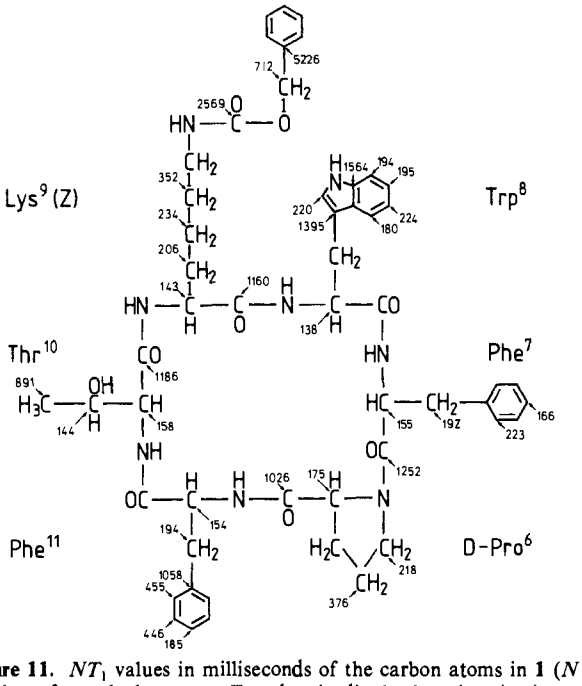

Figure 11. NT_1 values in milliseconds of the carbon atoms in **1** (N = number of attached protons, T_1 = longitudinal relaxation time).

carbons of the aromatic amino acid residues demonstrate also increased mobility due to rotation about the C^{α}–C^{β} bond. However, the NT_1 value for the β carbon of the Thr[3] residue is similar to the backbone NT_1 values. This supports the finding that the Thr-OH group is locked by hydrogen bonds. As usual, the mobility in the proline ring follows the order $\gamma > \delta > \alpha$.[57,91]

Considering the phenyl rings, the para carbons, which are not influenced by phenyl-ring rotation (about the C^{β}–C^{ipso} bond), exhibit an NT_1 value similar to that of the β carbons. By contrast, the ortho and meta carbon atoms have significantly longer relaxation times, because the orientation of the C–H bond vector is changing with the fast phenyl group rotation. In this respect, the Phe[2] residue seems to rotate more rapidly than the other aromatic side chains. Interestingly, the Trp[5] residue seems also to be quite rigid, as all protonated carbons have similar NT_1 values which are comparable to the values of the backbone carbons.

Conformation and Biological Activity

Hepatocytes are protected by the peptide hormone somatostatin against poisons such as ethanol, dimethyl sulfoxide, cysteamine, or phalloidin.[92] Recently, we synthesized a series of cyclic hexapeptides containing the partial sequence Phe[6] to Phe[11] of somatostatin in which the residues Phe[6], Trp[8], and Phe[11] were

(87) Loosli, H. R.; Kessler, H.; Oschkinat, H.; Weber, H. P.; Petcher, T. J.; Widmer, A. *Helv. Chim. Acta* **1985**, *68*, 682–703.
(88) Bats, J. W.; Fuess, H.; Kessler, H.; Schuck, R. *Chem. Ber.* **1980**, *113*, 520–530.
(89) Lyerla, J. R.; Levy, G. C. *Top. Carbon-13 NMR Spectrosc.* **1974**, *1*, 79–148.
(90) Woessner, D. E.; Snowden, B. S.; Meyer, G. H. *J. Chem. Phys.* **1969**, *50*, 719.
(91) Kessler, H.; Friedrich, A.; Krack, G.; Hull, W. E. *Peptides: Synthesis, Structure, Function*; Rich, D. M., Gross, E., Eds.; Pierce Chem. Comp.: Rockford, IL, 1981; pp 335–338.
(92) (a) Frimmer, M.; Petzinger, E. *Arzneim.-Forsch.* **1975**, *25*, 1423. (b) Frimmer, M. *Toxicol. Lett.* **1987**, *35*, 169–182.

systematically varied from the L to D configuration.[2,93] Although these compounds exhibited significant increase of cytoprotection activity as monitored by the phalloidin uptake of isolated hepatocytes, the surprising finding in these studies was the strongly increased activity of the retro-analogues of somatostatin.[64,93] In these peptides the endocrinic effects of the natural precursor are completely suppressed. Employing radioactive material, the cytoprotection was identified to be due to the inhibition of a multispecific transport system through the liver cell membrane.[94,95] Cytoprotective activity is not restricted to phalloidin and cholate uptake in liver cells but can also be employed to prevent taurocholate- or cerulein-induced pancreatitis in rats and duodenal ulcera induced by ethanol in rats.[9,96,97] In vivo studies were carried out with the peptide deprotected at the Lys side chain, whereas in vitro assays were performed with and without Z protection of the Lys residue. The Z-protected derivative turned out to be more active than the deblocked peptide.[95] It is long known that antamanide (**3**) exhibits a similar cytoprotective activity. To localize that part of **3** which is responsible for the biological activity, Wieland and co-workers synthesized more than 80 derivatives[11,12] of antamanide. In summary, they found that antamanide itself has the highest activity, and no defined "active region" could be localized. However, the phenylalanines, especially Phe[9] and Phe[10], could not be substituted by nonaromatic amino acids, and the manipulation at the Pro[7] and Pro[8] sites led to a dramatic decrease of activity.

Considering the activity of our retro-somatostatin derivatives as well as of antamanide and cyclolinopeptide,[10] we anticipate that the sequence of two adjacent aromatic amino acids flanked by proline would be the minimum requirement for high cytoprotective activity.[10,64] Hence, we synthesized two peptides which contain this moiety: *cyclo*(-D-Pro-Phe-Phe-Pro-Phe-Phe-) (**8**)[10] and *cyclo*(-Pro-Pro-Phe-Phe-Gly-) (**9**).[98] It turned out that analogue **8** exhibits cytoprotective activity higher than antamanide (see Table I), whereas the cyclic pentapeptide **9** is completely inactive. NMR investigations revealed that the conformation of peptide **9** in Me_2SO solution is unusual compared with other cyclic pentapeptides: it includes two adjacent cis peptide bonds about the proline residues, and the two L-phenylalanines are involved in a βII′ turn in $i + 1$ and $i + 2$ position[98] where normally β turns of type I are preferred in such sequences.[99,100]

In contrast, the X-ray analysis of the crystalline cyclic hexapeptide **8** yields a structure which is very similar to that of **1** in solution (Figure 7). This is not surprising since the constitutional similarities between **1** and **8** are high. The backbone involves a βI turn about Pro[4] and Phe[5] and a βII′ turn about D-Pro[1] and Phe[2]. This corresponds to the kind of turns expected from the chirality of these amino acids and the rules of a preferred position of a proline in the $i + 1$ position of β turns.[99] A trans conformation about both Phe-Pro bonds also follows.[99]

The structure of a peptide is not only determined by the backbone conformation but also the orientation of the side chains. Many conformational studies have shown that the rotamer distribution is preferentially shifted to a single rotamer the more "rigid" the backbone is. Hence, the side-chain conformation can be taken as an indicator for the rigidity of the molecule. In addition, the correct side-chain conformation should facilate binding to the receptor. Thus, when certain side-chain conformations are accompanied by high biological activity, it is probable that they adopt in solution the same conformation as in the receptor. In **1** the most populated conformation of Phe[2], Trp[5], and Phe[6] is identical with that of the corresponding aromatic amino acids in **8**. In addition, the different surrounding and the preference of intermolecular hydrogen bonding in the crystalline state[101] might well destroy common structural features. The equivalence of the conformations of **1** and **8** suggests that the conformations shown in Figure 7 are stable minima on the energetic hypersurface. Because both compounds are biologically strongly active, we think that this conformation is also close to the conformation of the molecule bound to the receptor. In antamanide, the side chain of Phe[9] is also bent over the Pro[8] ring in the crystal[102,103] and in solution.[104] Model building shows that the lipophilic space of the sequence Pro[8]-Phe[9] in antamanide is relatively similar to the Phe[6]-D-Pro[1] sequence in **1** although the peptide bond is reversed.

Conclusion

In this paper we have shown the conformational analysis of a highly potent cyclic hexapeptide by NMR analysis in solution. We have used rotating frame NOEs to measure distances between protons. Using these distances constrained MD calculation refinements are performed. The influence of the solvent environment is taken into account by reducing the charge of solvent-exposed NH protons. Homo- and heteronuclear coupling constants as well as chemical shift values and their temperature dependence and carbon relaxation times deliver additional information about the conformation and flexibility of the backbone and the side chains. A similar conformation was found for an analogue of the title compound in the crystalline state. Comparison of the conformation of the cyclic peptides with high or low activity in the inhibition of a hepatocytic transport system reveals common structural features related to this activity.

Experimental Section

The protected amino acids and deuterated derivatives were prepared as described in the literature. All intermediates were characterized by TLC, melting point, specific rotation, IR, and ^1H NMR.

TLC was performed on silica gel (Merck 254 plates) in the following systems (v/v): (A) 1-butanol/acetic acid/water, 3:1:1; (B) chloroform/methanol, 9:1; (C) chloroform/acetic acid/methanol, 92:3:5. Optical rotation was determined on a Perkin-Elmer polarimeter, Model 141, at the sodium D line. IR spectra were recorded on a Perkin-Elmer spectrometer, Type 257. Sephadex LH 20 was used for gel chromatography (eluent: methanol). HPLC was performed on a Beckman system (420 Controller, 110B Solvent Delivery Module) in the following systems (v/v): (D) methanol/water, 4:1; (E) acetonitrile/water, 7:3. The FAB–MS spectra were recorded on a VG ZAB-3HF spectrometer (ionization via ≈7-eV xenon atoms).

Proton and carbon spectra were recorded on Bruker spectrometers (WH 270, AM 300, AM 500) and processed on a Bruker data station with an Aspect 3000 computer and a 160-Mbyte B-DS 160F disk. A 19-mg sample of **1** in a 5-mm tube (0.7 mL Me_2SO, degassed) was used for the homonuclear, and a 250-mg sample of **1** in a 10-mm tube (3 mL Me_2SO, degassed) for the heteronuclear measurements. The spectra were recorded at 300 K.

DOF-COSY (300 MHz). Pulse sequence: $\pi/2_\phi$, t_1, $\pi/2_\phi$, Δ_1, $\pi/2$, aq; 1536 experiments of 16 scans each, relaxation delay 1.5 s, acquisition time for one scan 0.6 s, Δ_1 = 3 ms, size 4K, spectral width in F2 and F1 3400 Hz, zero filling to 8K in F2 and to 4K in F1, apodization in both dimensions with squared sinebell shifted by $\pi/4$.

E. COSY (300 MHz). Pulse sequence: $\pi/2_\beta$, t_1, $\pi/2_\beta$, $\pi/2$, aq; 1200 experiments, (β_0 = 20 scans, $\beta_1 = \beta_7$ = 16 scans, $\beta_2 = \beta_4 = \beta_6$ = 4 scans, $\beta_3 = \beta_5$ = 2 scans), weighting factors ($DC_0 = DC_2 = DC_4 = DC_6$ = 1, $DC_1 = DC_7$ = −1.067, $DC_3 = DC_5$ = −1.1716), relaxation delay 1.2 s, acquisition time for one scan 0.73 s, size 4K, spectral width in F2 and F1 2800 Hz, zero filling to 8K in F2 and to 4K in F1, Lorentz to Gauss multiplication in both dimensions (GB = 0.2, LB2 = −1, LB1 = −2).

ROESY (300 MHz). Pulse sequence: $\pi/2$, t_1, $(\beta - \tau)_n$, aq. Mixing with 180° pulses: 1200 experiments of 16 scans each, relaxation delay

(93) Rao, G. S.; Lemoch, H.; Kessler, H.; Damm, I.; Eiermann, V.; Koll, S.; Zarbock, J.; Usadel, K. H. *Klin. Wochenschr.* **1986**, *64*, 87–89.
(94) Ziegler, K.; Frimmer, M. *Klin. Wochenschr.* **1986**, *64*, 87–89.
(95) Kessler, H.; Haupt, A.; Frimmer, M.; Ziegler, K. *Int. J. Peptide Protein Res.* **1986**, *29*, 621–628.
(96) Rohr, G.; Keim, V.; Usadel, K. H. *Klin. Wochenschr.* **1986**, *64*, 90–92.
(97) Palitsch, K. D.; Schuler, H.; Schwedes, U.; Usadel, K. H. *Klin. Wochenschr.* **1986**, *64*, 93–96.
(98) Kessler, H.; Müller, A. *Justus Liebigs Ann. Chem.* **1986**, 1687–1704.
(99) Smith, J. A.; Pease, L. G. *CRC Crit. Rev. Biochem.* **1980**, *19*, 315–399.
(100) Gierasch, L. M.; Deber, C. M.; Madison, V.; Niu, C. H.; Blout, E. R. *Biochemistry* **1981**, *20*, 4730–4738.
(101) Kessler, H.; Zimmermann, G.; Förster, H.; Engel, J.; Oepen, G.; Sheldrick, W. S. *Angew. Chem., Ed. Engl. Int.* **1981**, *20*, 1053–1055.
(102) Karle, I. L. *J. Am. Chem. Soc.* **1977**, *99*, 5152–5154.
(103) Karle, I. L.; Duesler, E. *Proc. Natl. Acad. Sci. U.S.A.* **1977**, *74*, 2602–2606.
(104) Müller, A. Ph.D. Thesis, Frankfurt; Germany, 1986.

2.5 s, acquisition time for one scan 0.6 s, β = 16.8 μs, τ = 168 μs, n = 1082, total mixing time 200 ms, size 4K, spectral width in F2 and F1 3400 Hz, zero filling in F2 to 8K and in F1 to 4K, squared cosine multiplication in both dimensions.

Mixing with small flip angle pulses (17°): 800 experiments of 32 scans each, relaxation delay 2.5 s, acquisition time for one scan 0.51 s, β = 2.5 μs, τ = 25 μs, n = 7272, total mixing time 200 ms, size 4K, spectral width in F2 and F1 4000 Hz, zero filling in F2 to 8K and in F1 to 4K, squared cosine multiplication in both dimensions, automatic baseline correction with Bruker software.

NOESY (500 MHz). Pulse sequence: $\pi/2$, t_1, $\pi/2$, Δ_1, $\pi/2$, aq; 1280 experiments of 32 scans each, relaxation delay 2.5 s, acquisition time for one scan 0.43 s, Δ_1 = 250 ms, size 4K, spectral width in F2 and F1 4800 Hz, zero filling in F2 to 8K and in F1 to 4K, squared cosine multiplication in both dimensions.

H,C-COSY (270 MHz), aliphatic carbon resonances observed. Pulse sequence: $\pi/2$ (^{1}H), $t_1/2$, π (^{13}C), $t_1/2$, Δ_1, $\pi/2$ (^{1}H, ^{13}C), Δ_2, aq (^{13}C, ^{1}H-BB); 160 experiments of 192 scans each, relaxation delay 1.5 s, acquisition time for one scan 0.49 s, Δ_1 = 3.7 ms, Δ_2 = 2.5 ms, size 4K, spectral width in F2 4200 Hz, in F1 1800 Hz, zero filling to 8K in F2, exponential multiplication (line broadening of 1 Hz), zero filling to 0.5K in F1, squared cosine multiplication.

H,C-COSY (500 MHz), aromatic carbon resonances observed. Pulse sequence as described above; 160 experiments of 128 scans each, relaxation delay 1.5 s, acquisition time for one scan 1.37 s, Δ_1 = 3.1 s, Δ_2 = 2.1 s, size 8K, spectral width in F2 3000 Hz, in F1 400 Hz, zero filling to 16K in F2, exponential multiplication (line broadening of 0.4 Hz), zero filling to 0.5K in F1, squared cosine multiplication.

H,C-COLOC (300 MHz), carbonyl carbon resonances observed. Pulse sequence: $\pi/2$ (^{1}H), $t_1/2$, π (^{1}H, ^{13}C), $\Delta_1 - t_1/2$, $\pi/2$ (^{1}H, ^{13}C), Δ_2, aq (^{13}C, ^{1}H-BB); 144 experiments of 128 scans each, relaxation delay 1.83 s, acquisition time for one scan 1.83 s, Δ_1 = 25 ms, Δ_2 = 30 ms, size 1K, spectral width in F2 280 Hz, in F1 3000 Hz, zero filling to 2K in F2, exponential multiplication (line-broadening of 0.3 Hz), zero filling to 0.5 K in F1, sinebell multiplication.

H,C-COLOC (270 MHz), aromatic carbon resonances observed; 112 experiments of 256 scans each, relaxation delay 1.32 s, Δ_1 = 18 ms, Δ_2 = 21 ms, size 2K, spectral width in F2 2500 Hz, F1 3400 Hz, zero filling to 4K, exponential multiplication (line broadening of 1.2 Hz), zero filling to 0.5K in F1, sinebell multiplication.

T_1 relaxation times (300 MHz), aliphatic carbon resonances observed, pulse sequence: π, τ, $\pi/2$, aq (^{13}C, ^{1}H-BB); 10 experiments of 1024 scans each, relaxation delay 2.5 s, acquisition time for one scan 1.82 s, τ = (1, 10, 20, 50 ms; 0.1, 0.2, 0.3, 0.4, 0.5 s), size 16K, spectral width 4500 Hz, zero filling to 32K, exponential multiplication (line broadening of 0.3 Hz).

T_1 relaxation times (300 MHz), carbonyl and aromatic carbon resonances observed; 10 experiments of 400 scans each, relaxation delay 12.5 s, acquisition time for one scan 1.41 s, τ = (0.1, 0.2, 0.4, 0.6, 0.9, 1.2, 1.5, 2, 4, 8 s), size 16K, spectral width 5800 Hz, zero filling to 32K, exponential multiplication (line broadening of 0.4 Hz).

H,N-COSY (300 MHz), pulse sequence as H,C-COSY (note the different phase cycling due to the negative γ of nitrogen); 64 experiments of 800 scans each, relaxation delay 1 s, acquisition time for one scan 0.52 s, $\Delta_1 = \Delta_2$ = 5.4 ms, size 2K, spectral width in F2 2200 Hz, in F1 1420 Hz, zero filling in F2 to 4K, in F1 to 0.25K, exponential multiplication (line broadening of 3 Hz) in both dimensions.

^{15}N chemical shifts in Me_2SO, 300 K (external standard, formamide): 108.7 (Trp^5-NH$_{indole}$), 98.6 (Phe^2), 92.8 (Lys^4-NH$^\alpha$), 90.0 (Phe^6), 89.0 (Trp^5-NH$^\alpha$), 84.8 (Thr^3), 61.6 (Lys4-NH$^\epsilon$).

Molecular Dynamics Calculations. The calculations were performed on a VAX 8300 computer using the GROMOS program.[76] When performing MD calculations, the available kinetic energy allows the system to surmount barriers that are of the order of k_BT within a few picoseconds. But the higher the barrier, the more the MD simulation has to be extended in order to observe a transition. E.g., the cis/trans barrier in proline is too high to pass within a reasonable amount of time.[76,77,103,104] Therefore, it is recommendable to start with a structure not too far from the expected result. The starting structure for the simulation was based on the X-ray structure of the analogous cyclic hexapeptide **8**.[10] The potential function which describes the interaction between the atoms in the molecule reads:

$$V_{pot}(r_1,r_2,\ldots,r_n) = V_{bonds} + V_{angles} + V_{improper\ dihedrals} + V_{dihedrals} + V_{van\ der\ Waals} + V_{coulomb} + V_{distances}$$

Except for the last term this is a function generally applied to peptides.[105] The last term is included as a pseudopotential, $V_{distances} = 0.5K_{dc}(r_{ij} - r_{0ij})^2$ with a force constant K_{dc} = 1000 kJ·mol^{-1}·nm^{-2}. The lower bound potential was multiplicated by a facter 2 to avoid an overestimation of short distances in partially flexible systems. The distance restraints r_{0ij} between atoms i and j is taken from the set of experimental distances obtained from ROE data (ROESY experiment, Table VIII). In addition, N*H* temperature gradients were used in calculation ii to scale the charge of the different NH fragments (see Table IX). The refinement procedure performed is the same for both calculations. The crude initial structure was relaxed by performing 250 conjugate gradient energy minimization (EM) steps.[106] Then the proton–proton distances obtained from the NMR measurements were included in the calculation as distance restraints, and another 250 EM steps were performed. After the restrained EM a restrained MD run over 50 ps was started. The MD time step was 0.002 ps. Proceeding from a strong coupling of the molecule to a thermal bath of T_0 = 1000 K, the coupling was stepwise decreased during the first 10 ps: the temperature relaxation time increased from 0.01 to 0.1 ps.[107] In addition, the temperature of the thermal bath was scaled down to T_0 = 300 K after the first picosecond. The first 10 ps were used for the equilibration of the molecule. The time from 11 to 50 ps was used for averaging. All calculations were performed in vacuo. In addition, the shake routine was used to force distances between two bonded atoms fixed in a defined range.[108]

X-ray Structure Determination of *cyclo*(-D-Pro-Phe-Thr-Phe-Trp-Phe-) (7). Measurements were performed on an Enraf-Nonius CAD4 diffractometer with Cu Kα radiation (graphite monochromator). Crystals used for the experiments were sealed in glass capillaries together with a drop of mother liquor. Colorless transparent crystals were grown by equilibration from a saturated solution in acetone, methanol, and water. Two crystalline modifications were obtained.

1. Orthorhombic Modification. *cyclo*(-D-Pro-Phe-Thr-Phe-Trp-Phe-)·3H$_2$O, a = 9.115 (9), b = 20.626 (5) c = 25.361 (6) Å, V = 4768 (7) Å^3, Z = 4, space group $P2_12_12_1$, ρ_{calcd} = 1.227 g/cm^3. Crystal dimensions: 0.3 × 0.35 × 0.75 mm. Data in an octant of reciprocal space were measured up to 2θ = 100°. Reflection profiles were very broad owing to a poor crystal quality. Consequently a large scan width was used (ω scan, $\Delta\omega$ = 6°). Three standard reflections repeatedly remeasured remained stable; 2786 independent reflections were obtained of which 2175 with $I > 1\sigma(I)$ were used. An empirical absorption correction was made based on ψ scan.[109] The structure was determined by Patterson search techniques using the program PATSEE[110] and using the backbone fragment of *cyclo*(-D-Pro-Phe-Phe-Pro-Phe-Phe-) (**8**) as search fragment. The structure was completed by difference Fourier syntheses. H-atom positions at the main molecule were calculated assuming C–H and N–H distances of 0.98 Å. Only the hydroxyl proton at the Thr residue was taken from a difference Fourier synthesis. The H atom positions at the three water molecules could not be located. The structure was refined on F using unit weights. The non-H atoms were refined with anisotropic thermal parameters. The H atom positions were not varied. Refinement converged at $R(F)$ = 0.079, $wR(F)$ = 0.077. The final difference density showed a peak of 0.39 e/Å^3 which could represent a partially occupied fourth water molecule, but was otherwise featureless. The fractional atomic coordinates are given in Table XIII.

2. Monoclinic Modification. 2*cyclo*(-D-Pro-Phe-Thr-Phe-Trp-Phe-)·5H$_2$O·CH$_3$OH·CH$_3$COCH$_3$: a = 9.256 (3), b = 26.135 (5), c = 20.108 (5) Å, β = 91.41 (2)°, V = 4863 (4) Å^3, Z = 2, space group $P2_1$, ρ_{calcd} = 1.251 g/cm^3. Crystal dimensions: 0.1 × 0.35 × 0.65 mm. Crystals of the monoclinic modification were systematically twinned about 001. The crystal used had a main twin domain corresponding to 64% of the crystal volume. Only reflections belonging to the main domain were measured. Data in one quadrant of reciprocal space were measured up to 2θ = 100° using a ω scan ($\Delta\omega$ = 3°). Three standard reflections remeasured every 5500 s decreased 11% during data collection. All data were rescaled with respect to the standards; 5136 independent reflections were obtained of which 4791 with $I > 1\sigma(I)$ were used. An empirical absorption correction based on ψ scans was made.[109] The structure was determined by Patterson search techniques using the program PATSEE[110] and taking the backbone of the orthorhombic modification as search fragment. The resulting partial structure was expanded by tangent refinement and difference Fourier syntheses. Overlapping of reflection

(105) van Gunsteren, W. F.; Berendsen, H. J. C. *Biochem. Soc. Trans.* **1982**, *10*, 301–305.

(106) (a) Fletcher, R.; Reeves, C. M. *Comput. J.* **1964**, *7*, 149–154. (b) van Gunsteren, W. F.; Karplus, M. *J. Comput. Chem.* **1980**, *7*, 266–274.

(107) Berendsen, H. J. C.; Postma, J. P. M.; van Gunsteren, W. F.; DiNola, A.; Haak, J. R. *J. Chem. Phys.* **1984**, *81*, 3684–3690.

(108) van Gunsteren, W. F.; Berendsen, H. J. C. *Mol. Phys.* **1977**, *34*, 1311–1327.

(109) North, A. C. T.; Phillips, D. C.; Mathews, F. S. *Acta Crystallogr., Sect. A* **1968**, *24*, 351–359.

(110) Egert, E.; Sheldrick, G. M. *Acta Crystallogr., Sect. A* **1985**, *41*, 262–268.

Table XIV. Positional Parameters and Equivalent Values of Anisotropic Thermal Parameters of 7 (Monoclinic Modification)

atom	*x*	*y*	*z*	*B* (Å²)	atom	*x*	*y*	*z*	*B* (Å²)
				Molecule 1					
O1(Phe4)	0.7459 (8)	0.8914	0.4677 (5)	4.0 (2)	C1-4(Trp5)	1.156 (2)	0.8572 (6)	0.3594 (6)	4.2 (3)
O1(Trp5)	0.8775 (9)	0.7403 (4)	0.4856 (5)	5.4 (2)	C1-5(Trp5)	1.201 (2)	0.8805 (9)	0.3014 (9)	6.9 (5)
O1(Phe6)	0.6368 (9)	0.7805 (4)	0.6955 (5)	4.4 (2)	C1-6(Trp5)	1.330 (2)	0.904 (1)	0.299 (1)	8.1 (6)
O1(Pro1)	0.288 (1)	0.8322 (4)	0.6707 (5)	5.0 (3)	C1′(Phe6)	0.597 (1)	0.7536 (6)	0.6450 (7)	3.9 (3)
O1(Phe2)	0.488 (1)	0.9482 (4)	0.8038 (6)	6.1 (3)	C1$^{\alpha}$(Phe6)	0.709 (1)	0.7378 (5)	0.5964 (8)	4.2 (3)
O1(Thr3)	0.6455 (9)	0.8870 (5)	0.6188 (5)	5.5 (3)	C1$^{\beta}$(Phe6)	0.813 (2)	0.6978 (8)	0.6284 (9)	6.6 (5)
O1$^{\gamma}$(Thr3)	0.9692 (9)	0.9404 (4)	0.7523 (5)	4.8 (2)	C1-*i*(Phe6)	0.740 (2)	0.6507 (7)	0.657 (1)	6.2 (5)
N1(Phe4)	0.810 (1)	0.9506 (5)	0.6227 (6)	4.3 (3)	C1-*o*1(Phe6)	0.691 (2)	0.6432 (8)	0.721 (1)	7.6 (5)
N1(Trp5)	0.930 (1)	0.8730 (5)	0.5376 (5)	3.8 (3)	C1-*m*1(Phe6)	0.625 (2)	0.601 (1)	0.744 (1)	14.2 (7)
N1(Phe6)	0.788 (1)	0.7839 (4)	0.5743 (6)	3.8 (3)	C1-*p*(Phe6)	0.612 (3)	0.563 (1)	0.697 (1)	11.9 (8)
N1(Pro1)	0.4632 (9)	0.7403 (4)	0.6396 (5)	3.3 (2)	C1-*m*2(Phe6)	0.649 (3)	0.562 (1)	0.634 (2)	10.4 (8)
N1(Phe2)	0.384 (1)	0.8153 (4)	0.7742 (5)	3.5 (2)	C1-*o*2(Phe6)	0.717 (2)	0.6082 (9)	0.615 (1)	9.1 (6)
N1(Thr3)	0.603 (1)	0.8863 (4)	0.7486 (6)	3.9 (3)	C1′(Pro1)	0.344 (1)	0.8018 (7)	0.7116 (6)	4.3 (3)
N1-1(Trp5)	1.439 (1)	0.8849 (6)	0.4740 (7)	5.9 (4)	C1$^{\alpha}$(Pro1)	0.361 (1)	0.7464 (5)	0.6936 (6)	2.6 (3)
C1′(Phe4)	0.825 (1)	0.9019 (6)	0.5136 (7)	3.4 (3)	C1$^{\beta}$(Pro1)	0.217 (1)	0.7240 (6)	0.6665 (8)	4.2 (3)
C1$^{\alpha}$(Phe4)	0.805 (1)	0.9540 (5)	0.5504 (7)	3.7 (3)	C1$^{\gamma}$(Pro1)	0.266 (1)	0.6837 (8)	0.6181 (9)	6.6 (4)
C1$^{\beta}$(Phe4)	0.927 (1)	0.9929 (5)	0.5253 (8)	4.4 (3)	C1$^{\delta}$(Pro1)	0.396 (2)	0.7054 (7)	0.5852 (7)	4.9 (4)
C1-*i*(Phe4)	0.910 (2)	1.0005 (6)	0.4538 (8)	4.7 (4)	C1′(Phe2)	0.490 (1)	0.9042 (6)	0.7830 (7)	5.2 (3)
C1-*o*1(Phe4)	1.014 (2)	0.986 (1)	0.413 (1)	9.4 (6)	C1$^{\alpha}$(Phe2)	0.368 (1)	0.8671 (6)	0.8006 (7)	3.9 (3)
C1-*m*1(Phe4)	0.988 (2)	0.9949 (9)	0.341 (1)	8.3 (6)	C1$^{\beta}$(Phe2)	0.350 (2)	0.8610 (7)	0.8765 (7)	5.3 (4)
C1-*p*(Phe4)	0.881 (3)	1.014 (1)	0.317 (1)	11.1 (8)	C1-*i*(Phe2)	0.205 (2)	0.8418 (6)	0.8937 (8)	5.2 (4)
C1-*m*2(Phe4)	0.785 (3)	1.0352 (9)	0.359 (1)	10.2 (7)	C1-*o*1(Phe2)	0.097 (2)	0.8777 (6)	0.9109 (7)	5.2 (4)
C1-*o*2(Phe4)	0.800 (2)	1.0281 (9)	0.427 (1)	8.6 (6)	C1-*m*1(Phe2)	−0.042 (2)	0.8607 (7)	0.9250 (8)	5.6 (4)
C1-7(Trp5)	1.425 (2)	0.9107 (7)	0.351 (1)	6.5 (5)	C1-*p*(Phe2)	−0.068 (2)	0.8072 (9)	0.9214 (8)	7.2 (5)
C1′(Trp5)	0.870 (1)	0.7788 (7)	0.5210 (7)	4.9 (4)	C1-*m*2(Phe2)	0.036 (1)	0.7744 (8)	0.9071 (9)	6.7 (4)
C1$^{\alpha}$(Trp5)	0.964 (1)	0.8267 (5)	0.5025 (7)	3.1 (3)	C1-*o*2(Phe2)	0.172 (2)	0.7895 (8)	0.8949 (9)	6.1 (5)
C1$^{\beta}$(Trp5)	1.126 (1)	0.8107 (7)	0.5142 (7)	5.1 (4)	C1′(Thr3)	0.720 (1)	0.9163 (5)	0.6531 (7)	3.5 (3)
C1-3(Trp5)	1.230 (1)	0.8460 (5)	0.4860 (7)	3.5 (3)	C1$^{\alpha}$(Thr3)	0.718 (1)	0.9180 (5)	0.7264 (7)	3.4 (3)
C1-2(Trp5)	1.353 (1)	0.8573 (7)	0.5161 (8)	4.9 (4)	C1$^{\beta}$(Thr3)	0.862 (1)	0.9029 (6)	0.7638 (9)	5.1 (4)
C1-7a(Trp5)	1.372 (1)	0.8864 (5)	0.4114 (7)	3.8 (3)	C1$^{\gamma}$(Thr3)	0.920 (2)	0.8519 (8)	0.7411 (9)	5.8 (5)
C1-3a(Trp5)	1.242 (1)	0.8634 (8)	0.4166 (7)	4.9 (4)	H1–O$^{\gamma}$(Thr3)	0.9727	0.9512	0.7988	7
				Molecule 2					
O2(Phe4)	0.2829 (8)	1.0855 (3)	1.0233 (5)	3.6 (2)	C2-4(Trp5)	0.725 (2)	1.1553 (6)	1.1312 (8)	4.6 (3)
O2(Trp5)	0.3484 (9)	1.2319 (4)	1.0309 (5)	5.3 (2)	C2-5(Trp5)	0.795 (2)	1.1397 (8)	1.1887 (8)	6.2 (5)
O2(Phe6)	0.1162 (9)	1.1972 (4)	0.8218 (5)	4.7 (2)	C2-6(Trp5)	0.945 (2)	1.1222 (8)	1.1885 (9)	6.6 (5)
O2(Pro1)	−0.239 (1)	1.1619 (4)	0.8136 (5)	5.1 (2)	C2′(Phe6)	0.074 (1)	1.2270 (5)	0.8649 (7)	3.5 (3)
O2(Phe2)	−0.019 (1)	1.0416 (4)	0.6760 (6)	5.7 (3)	C2$^{\alpha}$(Phe6)	0.171 (1)	1.2417 (6)	0.9219 (7)	3.7 (3)
O2(Thr3)	0.1449 (9)	1.0855 (4)	0.8793 (5)	4.7 (2)	C2$^{\beta}$(Phe6)	0.239 (2)	1.2978 (7)	0.9114 (8)	5.4 (4)
O2$^{\gamma}$(Thr3)	0.459 (1)	1.0505 (4)	0.7343 (6)	5.6 (3)	C2-*i*(Phe6)	0.251 (1)	1.3083 (7)	0.8386 (9)	5.4 (4)
N2(Phe4)	0.339 (1)	1.0341 (5)	0.8656 (5)	4.1 (3)	C2-*o*1(Phe6)	0.351 (2)	1.2809 (9)	0.7996 (9)	7.5 (5)
N2(Trp5)	0.452 (1)	1.1141 (5)	0.9540 (6)	4.0 (3)	C2-*m*1(Phe6)	0.365 (2)	1.296 (1)	0.731 (1)	10.9 (7)
N2(Phe6)	0.277 (1)	1.2019 (4)	0.9312 (5)	3.6 (2)	C2-*p*(Phe6)	0.290 (2)	1.3304 (9)	0.705 (1)	10.6 (6)
N2(Pro1)	−0.0565 (9)	1.2496 (5)	0.8573 (5)	3.8 (3)	C2-*m*2(Phe6)	0.197 (2)	1.3596 (7)	0.743 (1)	8.6 (6)
N2(Phe2)	−0.114 (1)	1.1733 (4)	0.7194 (5)	3.3 (2)	C2-*o*2(Phe6)	0.181 (2)	1.3508 (7)	0.808 (1)	7.4 (5)
N2(Thr3)	0.084 (1)	1.0996 (4)	0.7497 (6)	3.9 (3)	C2′(Pro1)	−0.167 (1)	1.1882 (6)	0.7772 (7)	3.7 (3)
N2-1(Trp5)	0.982 (1)	1.1245 (5)	1.0088 (6)	4.7 (3)	C2$^{\alpha}$(Pro1)	−0.136 (1)	1.2443 (6)	0.7960 (7)	4.0 (3)
C2′(Phe4)	0.358 (1)	1.0783 (6)	0.9756 (7)	4.0 (3)	C2$^{\beta}$(Pro1)	−0.280 (2)	1.2738 (6)	0.8077 (8)	4.9 (4)
C2$^{\alpha}$(Phe4)	0.355 (1)	1.0268 (7)	0.9375 (8)	4.7 (4)	C2$^{\gamma}$(Pro1)	−0.252 (1)	1.3053 (7)	0.8656 (9)	5.8 (4)
C2$^{\beta}$(Phe4)	0.498 (1)	0.9959 (7)	0.9525 (8)	4.7 (4)	C2$^{\delta}$(Pro1)	−0.124 (1)	1.2846 (5)	0.9060 (7)	3.7 (3)
C2-*i*(Phe4)	0.530 (1)	0.9858 (6)	1.0237 (7)	4.6 (3)	C2′(Phe2)	−0.017 (1)	1.0850 (7)	0.7045 (8)	5.2 (4)
C2-*o*1(Phe4)	0.594 (2)	1.0219 (7)	1.0681 (8)	5.4 (4)	C2$^{\alpha}$(Phe2)	−0.135 (1)	1.1231 (5)	0.6909 (7)	3.3 (3)
C2-*m*1(Phe4)	0.630 (2)	1.0104 (7)	1.1310 (9)	6.4 (4)	C2$^{\beta}$(Phe2)	−0.167 (2)	1.1296 (8)	0.6145 (8)	5.7 (4)
C2-*p*(Phe4)	0.597 (2)	0.9679 (8)	1.1603 (9)	7.0 (5)	C2-*i*(Phe2)	−0.303 (1)	1.1561 (7)	0.6007 (7)	5.2 (4)
C2-*m*2(Phe4)	0.526 (2)	0.932 (1)	1.122 (1)	10.8 (7)	C2-*o*1(Phe2)	−0.434 (2)	1.130 (1)	0.5878 (9)	7.9 (6)
C2-*o*2(Phe4)	0.489 (2)	0.9417 (7)	1.0517 (8)	6.0 (4)	C2-*m*1(Phe2)	−0.567 (2)	1.1680 (9)	0.5767 (8)	6.9 (5)
C2-7(Trp5)	1.009 (2)	1.1190 (6)	1.1312 (8)	4.9 (4)	C2-*p*(Phe2)	−0.547 (2)	1.2217 (7)	0.5805 (9)	6.4 (4)
C2′(Trp5)	0.360 (1)	1.1996 (5)	0.9865 (7)	3.4 (3)	C2-*m*(Phe2)	−0.422 (2)	1.2391 (8)	0.5894 (9)	6.2 (4)
C2$^{\alpha}$(Trp5)	0.479 (1)	1.1608 (6)	0.9943 (7)	4.0 (3)	C2-*o*2(Phe2)	−0.304 (2)	1.2099 (6)	0.6002 (8)	5.1 (4)
C2$^{\beta}$(Trp5)	0.623 (1)	1.1832 (6)	0.9772 (7)	3.9 (3)	C2′(Thr3)	0.226 (1)	1.0603 (6)	0.8409 (7)	3.8 (3)
C2-3(Trp5)	0.752 (1)	1.1562 (5)	1.0042 (7)	3.7 (3)	C2$^{\alpha}$(Thr3)	0.209 (1)	1.0649 (7)	0.7666 (8)	4.9 (4)
C2-2(Trp5)	0.867 (1)	1.1423 (7)	0.9657 (8)	5.9 (4)	C2$^{\beta}$(Thr3)	0.340 (1)	1.0850 (6)	0.7307 (8)	4.1 (3)
C2-7a(Trp5)	0.941 (1)	1.1296 (5)	1.0735 (7)	3.7 (3)	C2$^{\gamma}$(Thr3)	0.394 (1)	1.1389 (5)	0.7558 (8)	4.2 (3)
C2-3a(Trp5)	0.794 (1)	1.1462 (5)	1.0722 (7)	3.4 (3)	H2–O$^{\gamma}$(Thr3)	0.4316	1.0215	0.7148	7
				Solvent					
O(W1)	0.093 (1)	0.5073 (5)	0.1476 (6)	7.3 (3)	O(acetone)	0.922 (3)	0.413 (1)	0.903 (2)	24 (1)
O(MeOH)	1.392 (2)	0.9859 (7)	0.6309 (9)	11.5 (5)	C1(acetone)	0.943 (3)	0.458 (1)	0.902 (2)	14.7 (9)
O(W2)	0.423 (1)	0.2477 (6)	0.1592 (6)	7.8 (3)	C2(acetone)	0.851 (3)	0.490 (2)	0.851 (2)	14 (1)
O(W3)	1.154 (1)	0.9219 (4)	0.6444 (5)	5.9 (3)	C3(acetone)	1.019 (4)	0.486 (2)	0.961 (2)	14 (1)
O(W4)	0.340 (1)	0.5689 (6)	0.1611 (6)	7.3 (3)	C(MeOH)	1.371 (4)	1.002 (2)	0.556 (2)	20 (1)
O(W5)	0.081 (1)	1.2352 (5)	0.6479 (5)	7.0 (3)					

profiles from the twin domains was most serious for reflections with $h = 1$. Thus these reflections were excluded from the structure refinement. Reflections with $h = 0$ (where both twins coincide) were treated with a separate scale factor. H atoms at the main molecules were placed at calculated positions and were not refined. H atom positions at the Thr hydroxyl groups were taken from difference syntheses. H-atom positions

Table XV. Bond Distances (Å) and Angles (Deg) in the Backbone of **7**

D-Pro[1]	Phe[2]	Thr[3]	Phe[4]	Trp[5]	Phe[6]
N_i–$C^{\alpha}{}_i$[a] [Å]					
1.473 (10)	1.450 (9)	1.492 (10)	1.411 (10)	1.442 (10)	1.461 (10)
1.47 (2)	1.46 (2)	1.43 (2)	1.46 (2)	1.44 (2)	1.48 (2)
1.43 (2)	1.44 (2)	1.50 (2)	1.46 (2)	1.48 (2)	1.44 (2)
$C^{\alpha}{}_i$–C'_i [Å]					
1.500 (11)	1.563 (12)	1.509 (12)	1.538 (11)	1.549 (12)	1.528 (11)
1.50 (2)	1.54 (2)	1.47 (2)	1.56 (2)	1.57 (2)	1.50 (2)
1.54 (2)	1.50 (2)	1.50 (2)	1.55 (2)	1.50 (2)	1.49 (2)
C'_i–O_i [Å]					
1.230 (9)	1.221 (10)	1.270 (11)	1.219 (10)	1.249 (9)	1.221 (9)
1.24 (2)	1.22 (2)	1.23 (2)	1.20 (2)	1.24 (2)	1.28 (2)
1.22 (2)	1.27 (2)	1.27 (2)	1.21 (2)	1.24 (2)	1.24 (2)
C'–N_{i+1} [Å]					
1.314 (10)	1.316 (11)	1.348 (12)	1.375 (10)	1.319 (10)	1.381 (11)
1.35 (2)	1.35 (2)	1.38 (2)	1.31 (2)	1.34 (2)	1.29 (1)
1.33 (2)	1.34 (2)	1.33 (2)	1.36 (2)	1.34 (2)	1.35 (2)
N_i–$C^{\delta}{}_i$ [Å]					
1.476 (10)					
1.54 (2)					
1.49 (2)					
C'_{i-1}–N_i–$C^{\alpha}{}_i$ [deg]					
117.6 (6)	124.0 (7)	121.2 (7)	120.8 (8)	116.7 (7)	118.2 (7)
123 (1)	123 (1)	124 (1)	119 (1)	118 (1)	117 (1)
120 (1)	124 (1)	120 (1)	120 (1)	120 (1)	121 (1)
N_i–$C^{\alpha}{}_i$–C'_i [deg]					
114.1 (7)	115.4 (7)	111.2 (8)	113.4 (7)	115.1 (7)	105.8 (7)
111 (1)	115 (1)	109 (1)	115 (1)	115 (1)	109 (1)
113 (1)	116 (1)	109 (1)	112 (1)	113 (1)	108 (1)
N_i–$C^{\alpha}{}_i$–$C^{\beta}{}_i$ [deg]					
102.6 (7)	109.8 (7)	108.7 (7)	108.4 (8)	110.0 (7)	110.9 (8)
105 (1)	106 (1)	109 (1)	110 (1)	112 (1)	112 (1)
104 (1)	108 (1)	108 (1)	109 (1)	109 (1)	114 (1)
C'_i–$C^{\alpha}{}_i$–$C^{\beta}{}_i$ [deg]					
110.7 (8)	109.7 (7)	114.0 (8)	111.1 (7)	104.2 (7)	108.4 (8)
111 (1)	113 (1)	116 (1)	108 (1)	106 (1)	110 (1)
111 (1)	112 (1)	116 (1)	110 (1)	111 (1)	111 (1)
O_i–C'_i–$C^{\alpha}{}_i$ [deg]					
119.4 (8)	118.9 (9)	119 (1)	123.6 (8)	117.5 (8)	122.0 (9)
120 (1)	120 (1)	124 (1)	119 (1)	118 (1)	118 (1)
120 (1)	121 (1)	121 (1)	121 (1)	117 (1)	121 (1)
O_i–C'_i–N_{i+1} [deg]					
124.8 (8)	124.4 (9)	120.5 (9)	121.4 (8)	124.3 (8)	120.5 (9)
123 (2)	121 (1)	120 (1)	126 (1)	125 (2)	118 (1)
126 (1)	124 (1)	121 (1)	122 (1)	121 (1)	120 (1)
$C^{\alpha}{}_i$–C'_i–N_{i+1} [deg]					
115.8 (8)	116.7 (9)	121.0 (9)	114.8 (8)	118.1 (8)	117.1 (8)
117 (1)	119 (1)	116 (1)	115 (1)	116 (1)	123 (1)
115 (1)	115 (1)	118 (1)	116 (1)	121 (1)	120 (1)
D-Pro[1]	$C'_{i-1}N_iC^{\delta}{}_i$		$C^{\alpha}{}_iN_iC^{\delta}{}_i$		
	128.8 (8)		113.2 (7)		
	126 (1)		109.3 (9)		
	126 (1)		114 (1)		

[a] First entry, orthorhombic modification; second entry, monoclinic modification, molecule 1; third entry, monoclinic modification, molecule 2.

Table XVI. Conformation Angles (Deg) in the Crystal Structures of **7**

	Φ	ψ	ω	χ_1		χ_2	
D-Pro[1]	60 (1)[a]	−122 (1)	−178 (1)	27 (1)		−37 (1)	
	62 (2)	−118 (1)	−177 (1)	29 (1)		−38 (1)	
	58 (2)	−121 (1)	−177 (1)	17 (2)		−21 (2)	
Phe[2]	−84 (1)	3 (2)	179 (1)	−76 (1)		85 (2)	−94 (1)
	−83 (1)	−3 (2)	176 (1)	−75 (2)		86 (2)	−96 (2)
	−96 (1)	10 (2)	−179 (1)	−66 2)		86 (2)	−95 (2)
Thr[3]	−127 (1)	176 (1)	−174 (1)	−167 (1)	69 (1)		
	−118 (1)	171 (1)	−174 (1)	−168 (1)	72 (2)		
	−131 (1)	−175 (1)	−177 (1)	−170 (1)	66 (2)		
Phe[4]	−51 (2)	−51 (1)	−171 (1)	180 (1)		74 (2)	−105 (2)
	−53 (2)	−45 (2)	−174 (1)	−174 (1)		73 (2)	−117 (2)
	−57 (2)	−51 (1)	−170 (1)	180 (1)		95 (2)	−80 (2)
Trp[5]	−84 (1)	−16 (2)	−174 (1)	−73 (1)		124 (1)	−61 (2)
	−85 (1)	−11 (2)	−174 (1)	−66 (2)		142 (1)	−57 (2)
	−78 (2)	−26 (2)	−175 (1)	−75 (2)		130 (2)	−60 (2)
Phe[6]	−164 (1)	139 (1)	167 (1)	173 (1)		84 (2)	−96 (2)
	−166 (1)	129 (1)	167 (1)	176 (1)		90 (2)	−90 (2)
	−167 (1)	161 (1)	166 (1)	94 (1)		122 (2)	−68 (2)

[a] First entry, orthorhombic modification; second entry, monoclinic modification, molecule 1; third entry, monoclinic modification, molecule 2.

Table XVII. Hydrogen Bonding in the Crystals of **7**

orthorhombic modification:

D - H.... A		D-H [Å]	H..A [Å]	D..A [Å]	D-H-A [°]	symmetry
Phe^4-NH	OC-Phe^2	1.00	2.07	2.95(1)	146	-0.5+x 0.5-y 1.0-z
Phe^4-NH	O$^\gamma$-Thr^3	1.00	2.32	2.96(1)	121	x y z
Trp^5-NH	O(W3)	1.01	2.38	3.31(1)	154	-1.0+x y z
Trp^5-N1	OC-Phe^4	1.01	1.99	2.84(1)	140	-1.0+x y z
Phe^2-NH	O(W1)	1.00	1.93	2.89(1)	161	-x 0.5+y 0.5-z
Thr^3-NH	OC-Phe^6	1.00	2.03	3.00(1)	165	x y z
Thr^3-O$^\gamma$H	O(W2)	0.99	1.86	2.77(1)	152	x y z

possible hydrogen bonds involving the hydrate groups:

O..... ..O		O ....O	symmetry
(W1)-O	OC-Trp^5	2.71(1)	x y z
(W2)-O	OC-Thr^3	3.13(1)	-0.5+x 0.5-y 1.0-z
(W2)-O	O(W3)	2.72(1)	-0.5+x 0.5-y 1.0-z
(W3)-O	OC-D-Pro^1	2.68(1)	x y z
(W3)-O	O$^\gamma$-Thr^3	2.85(1)	1.0+x y z

monoclinic modification (molecule-1, molecule-2):

D-H..... A		D-H [Å]	H..A [Å]	D. A [Å]	D-H-A [°]	symmetry
Phe^4-N1H	O2C-Phe^2	0.99	2.10	3.04(2)	157	1.0+x y z
Phe^4-N1H	O1$^\gamma$-Thr^3	0.99	2.39	2 97(2)	117	x y z
Trp^5-N1H	O(W3)	1.00	2.27	3.21(2)	156	x y z
Trp^5-N11	O1C-Phe^4	0.99	2.05	2.86(1)	137	1.0+x y z
Phe^6-N1H	O1C-Thr^3	0.98	2.22	3.14(2)	155	x y z
Phe^2-N1H	O(W2)	0.99	1.90	2.83(2)	155	1 0-x 0 5+y 1.0-z
Thr^3-N1H	O1C-Phe^6	1.01	2.00	2.98(2)	165	x y z
Thr^3-O$^\gamma$1H	O(W1)	0.98	1.93	2.74(2)	139	1.0-x 0.5+y 1.0-z
Phe^4-N2H	O1C-Phe^2	1.00	2.08	2.93(2)	142	x y z
Phe^4-N2H	O2$^\gamma$-Thr^3	1.00	2.25	2.92(2)	123	x y z
Trp^5-N2H	O(W4)	0.98	2.33	3.27(2)	158	1 0-x 0.5+y 1.0-z
Trp^5-N21	O2C-Phe^4	0.98	2.08	2.97(1)	149	1.0+x y z
Phe^6-N2H	O2C-Phe^6	1.00	2.24	2.63(1)	102	x y z
Phe^2-N2H	O(W5)	0.99	1.86	2.84(2)	172	x y z
Thr^3-N2H	O2C-Phe^6	0.98	1.98	2.95(2)	165	x y z
Thr^3-O2$^\gamma$H	O(MeOH)	0.89	1.95	2.74(2)	147	-1.0+x y z

possible hydrogen bonds involving the solvent molecules:

O.....O		O.....O	symmetry
(W1)-O	O(W4)	2.80(2)	x y z
(W1)-O	O2C-Thr^3	3.04(2)	-x -0.5+y 1-z
(MeOH)-O	O(W3)	2.78(2)	x y z
(W2)-O	O2C-Trp^5	2.69(2)	x -1+y -1+z
(W3)-O	O1C-D-Pro^1	2.70(2)	1+x y z
(W3)-O	O1$^\gamma$-Thr^3	2.84(2)	x y z
(W4)-O	O2C-D-Pro^1	2.65(2)	-x -0.5+y 1-z
(W4)-O	O2$^\gamma$-Thr^3	2.82(2)	1-x -0.5+y 1-z
(W5)-O	O1C-Trp^5	2.72(2)	1-x 0.5+y 1-z

at the solvent molecules could not be located. The two independent molecules were refined in alternating cycles. The structure was refined on F using unit weights to $R(F) = 0.094$ and $wR(F) = 0.100$. The final difference density was less than 0.3 e/Å^3. The fractional atomic coordinates are reported in Table XIV.

The calculations were performed with the SDP program system.[111] The main bond distances and angles in the two crystal structures are given in Table XV, the main conformation angles in Table XVI. Table XVII contains the observed hydrogen bond distances. Lists of structure factors of both crystals can be obtained from the authors.

Boc-Trp-Phe-D-Pro-Phe-Thr-Lys(*Z*)-O-CH$_2$-C$_6$H$_4$-Polymer. Boc-Lys(Z)-OH was esterified to 3.0 g of hydroxymethylated resin by the action of 2-dimethylaminopyridine and dicyclohexylcarbodiimide within 3 h; the unreacted hydroxyl groups of the resin were blocked via benzoylation (benzoyl chloride, pyridine). The title hexapeptide was assembled by sequential addition of Boc-Thr-OH, Boc-Phe-OH, Boc-D-Pro-OH, Boc-Phe-OH, and Boc-Trp-OH following the cycle of operations illustrated in Table II. Completion of each coupling was checked by a chloranil color test. Finally, the resin was washed (CH_2Cl_2, methanol) and dried in vacuo to obtain 2.4 g of peptide (0.77 mmol/g of resin). The synthesis of the isotopic isomers was carried out by the same procedure in comparable amount.

Table XVIII. ^{1}H Chemical Shifts (δ), and Coupling Constants of *cyclo*(-D-Pro^1-Phe^2-Thr^3-Phe^4-Trp^5-Phe^6-) (**7**) in Me_2SO Solution at 300 K Recorded at 270-MHz Spectrometer Frequency

	D-Pro^1	Phe^2	Thr^3	Phe^4	Trp^5	Phe^6
NH		8.75	7.83	8.12	7.50	7.10
H$^\alpha$	4.09	4.35	4.54	3.95	4.40	4.64
H$^{\beta pro\text{-}S}$	1.45	3.33		2.56	3.25	2.80
H$^{\beta pro\text{-}R}$	1.63	2.75	4.40		3.03	3.24
H$^{\gamma pro\text{-}S}$	1.79		1.21			
H$^{\gamma pro\text{-}R}$	1.29					
H$^{\delta pro\text{-}S}$	2.62					
H$^{\delta pro\text{-}R}$	3.40					
OH			5.19			
J(NH,H$^\alpha$) [Hz]		8.8	9.5	3.9	8.8	5.8
J(H$^\alpha$,H$^{\beta pro\text{-}S}$) [Hz]		3.0			4.2	9.0
J(H$^\alpha$,H$^{\beta pro\text{-}R}$) [Hz]		11.7	3.7		10.5	4.5
$-\Delta\delta/\Delta T$ [ppb/K]		5.0	2.4	3.0	2.0	1.0

[a] Coupling constants determined via DISCO,[47-49] assignments of diastereotopic β protons of the aromatic amino acids via COLOC;[33-35,68-70] the stereospecific assignment of the D-Pro^1 protons was done in comparison with compound **1**.

Boc-Trp-Phe-D-Pro-Phe-Thr-Lys(Z)-N$_2$H$_3$. To a suspension of 5.4 g of Boc-Trp-Phe-D-Pro-Phe-Thr-Lys(Z)-O-CH$_2$-C$_6$H$_4$-polymer in 100 mL of dry dimethylformamide (DMF), 10 mL of anhydrous hydrazine was added; the mixture was shaken vigorously. After 6 h, the residual solid was filtered and the solvents were removed under reduced pressure. Purification by gel chromatography yielded 1950 mg (78% of theory) of linear hexapeptide: R_f(A) 0.81, R_f(B) 0.44; mp 160–166 °C; $[\alpha]^{20}_D$ −22.5° (c 0.3, MeOH).

***cyclo*(-D-Pro-Phe-Thr-Lys(Z)-Trp-Phe-) (1).** Boc-Trp-Phe-D-Pro-Phe-Thr-Lys(Z)-N$_2$H$_3$ (1.1 g) was deblocked with 5 mL of trifluoroacetic acid (TFA) in 10 min. The resolved TFA salt was added under vigorous stirring into 200 mL of dry ether, and the resulting solid was collected and dried. Without further purification the solid was dissolved in 5 mL of dry DMF and cooled to −20 °C. To the solution 0.4 mL of concentrated HCl was added. After warming up to −15 °C 0.25 mL of isoamyl nitrite was added. The mixture was left at −10 °C for 60 min. The formation of the azide was monitored by IR spectra. After completion the reaction mixture was diluted with 1000 mL of dry precooled (−18 °C) DMF, neutralized with 0.75 mL of *N*-methylmorpholine, and placed in a freezer at −18 °C for 2 days. After further 2 days at 5 °C, the solution was warmed up and kept overnight at room temperature; 200 mL of water and 20 g of mix-bed resin (E. Merck, No. 4836) were introduced into the mixture which was stirred for 6 h. The resin was separated by filtration and the solvents were removed under reduced pressure. The oily cyclopeptide was purified by gel chromatography and subsequent HPLC (reversed-phase column).

1 (292 mg; 32% of theory): R_f(A) 0.81, R_f(B) 0.40; mp >200 °C; $[\alpha]^{20}_D$ −18.7° (c 0.25, MeOH); FAB-MS (MH+) 942.

4 (234 mg; 25% of theory): R_f(A) 0.82, R_f(B) 0.41; mp 190–200 °C; $[\alpha]^{20}_D$ −19.0° (c 0.4, MeOH); FAB-MS (MH+) 944.

5 (114 mg; 24% of theory): R_f(A) 0.79, R_f(B) 0.39; mp 190–200 °C; $[\alpha]^{20}_D$ −16.8° (c 0.3, MeOH); FAB-MS (MH+) 944.

6 (207 mg; 22% of theory): R_f(A) 0.80, R_f(B) 0.38; mp 190–200 °C; $[\alpha]^{20}_D$ −17.9° (c 0.35, MeOH); FAB-MS (MH+) 944.

cyclo(-D-Pro-Phe-Thr-Lys(Z)-(*R*,*R*)-(α,β-^{2}H)-Trp-Phe-) (137 mg; 29% of theory): R_f(A) 0.82, R_f(B) 0.36; mp 190–200 °C; $[\alpha]^{20}_D$ 10.5° (c 0.45, MeOH); FAB-MS (MH+) 944. NMR data will be published elsewhere.

cyclo(-D-Pro-Phe-Thr-Phe-Trp-Phe-) (**7**) (295 mg; 36% of theory): R_f(A) 0.84, R_f(B) 0.40; mp >200 °C; $[\alpha]^{20}_D$ −12.3° (c 0.2, MeOH); FAB-MS (MH+) 826. ^{1}H NMR chemical shifts are given in Table XVIII.

Acknowledgment. Financial support by the Deutsche Forschungsgemeinschaft and the Fonds der chemischen Industrie is gratefully acknowledged. We are indepted to Dr. W. van Gunsteren and J. Lautz for introduction in the use of GROMOS and many helpful comments. The computer facilities of the Institut der Organischen Chemie were available by a grant from the Bundesministerium für Forschung und Technologie. The sample

(111) Structure Determination Package, Enraf-Nonius, Delft, Holland, 1985.

(112) Wüthrich, K.; Billeter, M.; Braun, W. *J. Mol. Biol.* **1983**, *196*, 949–961.

for heteronuclear NMR investigations were kindly provided by Dr. A. Haupt, M. Klein, M. Krapp, and M. Schudok.

Supplementary Material Available: ^1H z-filtered 1D-COSY spectrum of **1**, two H,C-COSY spectra of **1** (aliphatic carbons or aromatic carbons are observed), two sections of the E.COSY spectrum of **1**, and table of general displacement parameter expressions for the orthorhombic modification and the monoclinic modifications of **7** (8 pages). Ordering information is given on any current masthead page.

Heteronuclear Chemical-Shift Correlations of Silanol Groups Studied by Two-Dimensional Cross-Polarization/Magic Angle Spinning NMR

Alexander J. Vega

Contribution No. 4350 from the E. I. du Pont de Nemours and Company, Central Research and Development Department, Experimental Station, Wilmington, Delaware 19898.
Received March 30, 1987

Abstract: A two-dimensional ^1H-^{29}Si magic-angle-spinning (MAS) NMR experiment is proposed as a method to characterize peaks in conventional proton MAS spectra of surface species on silicas and zeolites. Mixing is achieved by cross polarization. The 2D spectra identify the protons that are rigidly bound to silicon atoms in the substrate. The application of heteronuclear or homonuclear decoupling is not necessary, as sample spinning is sufficient to suppress the effects of dipolar interactions in the systems of interest. The criteria for proton line narrowing by MAS and for effective cross polarization are discussed. The assignment of proton signals is further aided by proton MAS spectra obtained following a spin-lock pulse and by ^{29}Si MAS spectra taken with varying cross-polarization periods. The method is demonstrated in anhydrous samples of H-rho and NH_4-rho zeolites. It is shown that the 2D method identifies the minor proton component which is the single source of cross polarization in a hydrated form of Ca,Na-A zeolite. In the fully hydrated form of H-rho, new proton and silicon species are revealed and the interconnectivity of the various sample components is brought out. Finally, a homonuclear 2D proton experiment was evaluated for the detection of proton spin exchange that could hinder the interpretation of heteronuclear correlations, but the results were inconclusive in the present application.

Proton magic angle spinning (MAS) has been used extensively in recent years to characterize surface hydroxyls on silicas,[1-4] aluminosilicates,[4,5] and zeolites.[2,6-16] With a few exceptions,[1,6] well-resolved chemical-shift spectra were routinely obtained without the simultaneous application of line-narrowing multiple pulse schemes which would suppress proton-proton dipolar interactions.[17,18] This is possible because the dipolar interactions in these samples are so weak that they can be averaged out by sample rotations with speeds of only a few kilohertz.[19]

The chemical information directly revealed by the proton resonance frequencies concerns in particular the acidity of hydroxyl groups.[4,11,12] Further structural identification of proton signals is generally based on an a priori knowledge of the sample chemistry or on the response of the spectrum to the adsorption of deuterated molecules.[1-4] Among the types of structural features that need to be distinguished are bridging and terminal hydroxyls, single and geminal hydroxyls, AlOH and SiOH, and hydrogen bonding, but the amount of information contained in the chemical shifts of the fairly wide proton MAS peaks is often insufficient to identify all the various proton species. On the other hand, additional spectroscopic information can sometimes be deduced from the spinning-sideband intensities, which indicate anisotropic dipolar interactions,[14,15] or from the extent to which the sidebands are affected by partial deuteration, which helps distinguish homonuclear from heteronuclear dipole interactions.[14,15] Furthermore, the ^{29}Si line shape obtained by ^1H-^{29}Si cross-polarization (CP/MAS)[20] with short contact times reveals the ^{29}Si subspectrum of the silicon sites that are in the proximity of a hydroxyl group.[3,14,15] The results presented in this paper suggest that an extension of the latter technique to two-dimensional (2D) spectroscopy can contribute significantly to the assignment of multiple proton MAS peaks, in that it allows the identification of the proton species that interact most strongly with the silica lattice.

In this paper we present 2D CP/MAS ^1H-^{29}Si results of some zeolite samples containing proton species with varying structural and dynamical properties. The anhydrous NH_4 and H forms of zeolite rho serve as examples to demonstrate the method, although actual spectra are only shown for the latter. The 2D spectrum

(1) Rosenberger, H.; Ernst, H.; Scheler, G.; Jünger, I.; Sonnenberger, R. *Z. Phys. Chem. (Leipzig)* **1982**, *263*, 846.
(2) Freude, D.; Hunger, M.; Pfeifer, H. *Chem. Phys. Lett.* **1982**, *91*, 307.
(3) Köhler, J.; Chase, D. B.; Farlee, R. D.; Vega, A. J.; Kirkland, J. J. *J. Chromatogr.* **1985**, *352*, 275.
(4) Pfeifer, H.; Freude, D.; Hunger, M. *Zeolites* **1985**, *5*, 274.
(5) Hunger, M.; Freude, D.; Pfeifer, H.; Bremer, H.; Jank, M.; Wendlandt, K. P. *Chem. Phys. Lett.* **1983**, *100*, 29.
(6) Freude, D.; Fröhlich, T.; Hunger, M.; Pfeifer, H.; Scheler, G. *Chem. Phys. Lett.* **1983**, *98*, 263.
(7) Scholle, K. F. M. G. J.; Veeman, W. S.; Post, J. G.; van Hoof, J. H. C. *Zeolites* **1983**, *3*, 214.
(8) Scholle, K. F. M. G. J.; Kentgens, A. P. M.; Veeman, W. S.; Frenken, P.; van der Velden, G. P. M. *J. Phys. Chem.* **1984**, *88*, 5.
(9) Freude, D.; Hunger, M.; Pfeifer, H.; Scheler, G.; Hoffmann, J.; Schmitz, W. *Chem. Phys. Lett.* **1984**, *105*, 427.
(10) Kasai, P. H.; Jones, P. M. *J. Mol. Catal.* **1984**, *27*, 81.
(11) Mastikhin, V. M.; Mudrakovskii, I. L.; Kotsarenko, N. S.; Karakchiev, L. G.; Pelmenshchikov, A. G.; Zamaraev, K. I. *React. Kinet. Catal. Lett.* **1984**, *27*, 47.
(12) Freude, D.; Hunger, M.; Pfeifer, H.; Schwieger, W. *Chem. Phys. Lett.* **1986**, *128*, 62.
(13) Fischer, R. X.; Baur, W. H.; Shannon, R. D.; Staley, R. H.; Vega, A. J.; Abrams, L.; Prince, E. *J. Phys. Chem.* **1986**, *90*, 4414.
(14) Vega, A. J.; Luz, Z. *J. Phys. Chem.* **1987**, *91*, 365.
(15) Luz, Z.; Vega, A. J. *J. Phys. Chem.* **1987**, *91*, 374.
(16) Lohse, U.; Löffler, E.; Hunger, M.; Stöckner, J.; Patzelova, V. *Zeolites* **1987**, *7*, 11.
(17) Gerstein, B. C. *Phil. Trans. R. Soc. London, Ser. A* **1981**, *299*, 521.
(18) Scheler, G.; Haubenreiser, U.; Rosenberger, H. *J. Magn. Reson.* **1981**, *44*, 134.
(19) Eckman, R. *J. Chem. Phys.* **1982**, *76*, 2767.
(20) Engelhardt, E.; Lohse, U.; Samoson, A.; Mägi, M.; Tarmak, M.; Lippmaa, E. *Zeolites* **1982**, *2*, 29. Nagy, J. B.; Gabelica, Z.; Derouane, E. G. *Chem. Lett.* **1982**, 1105.

0002-7863/88/1510-1049$01.50/0